

### Politecnico di Torino

Corso di Laurea Magistrale in Georesources and Geoenergy Engineering
A.A. 2024/2025

# Comparison of Three Saturation Methods for Rock Samples Used in Laboratory Petrophysical Analysis

Relatore:

Prof. Francesca Verga

Correlatore:

Dr. Costanzo Peter

Candidato:

Miguel Augusto Medina Gomez

# Acknowledgments

I would like to express my sincere appreciation to Prof. Francesca Verga, whose seriousness, high standards and unmistakable presence pushed me to do my best. Her rigor shaped the quality of this thesis and the way I now approach scientific work. My gratitude also goes to Dr. Costanzo Peter, whose calm guidance and constant availability made the laboratory feel navigable. His support was essential for every stage of this project. I am also thankful to the Politecnico di Torino for providing the environment in which this work could grow.

I would also like to thank Mauricio González, who many years ago opened the door to petrophysics for me and practically taught me everything I know about laboratory work. His early encouragement, his patience, and the way he shared his excitement for pore systems and fluid behavior planted the curiosity that eventually led me here.

To my friends in Torino, thank you for accompanying the version of me who talked about rock samples, fittings and capillary forces as if they were dramatic plot twists. You turned this city into a home with dinners, coffees, laughter and quiet company, and you let me be your unofficial geology professor, which genuinely made this journey brighter.

To my friends in Colombia, ustedes vivieron otra tesis completamente distinta, la de mi vida emocional. Thank you for the video calls at impossible hours, por el chisme, las risas, los "cuenta bien" y el cariño constante desde otra latitud. You kept me grounded even from afar.

To Manila and Nara, my two furry research assistants, thank you for sitting on my drafts, interrupting my spirals and bringing warmth to every day. This thesis carries your pawprints.

To the person who shared this whole thesis season with me, grazie. Working side by side, taking breaks for games, a series or something warm to eat, your "hai mangiato?" messages, the chocolates, the breakfasts and the gentle way you convinced me to keep working from the bed made everything feel strangely safe. There was a warmth in those days, unmistakably Italian, steady and kind, that made this journey lighter and far more human.

To my family, que han estado conmigo desde siempre incluso cuando la vida me llevó lejos, gracias por creer en mí con una constancia que no se parece a nada más. Ustedes son mi raíz, mi fuerza y mi recordatorio de que los sueños se construyen con trabajo, pero también con amor.

You taught me humility, resilience and the quiet truth that progress, much like permeability in tight rocks, often increases in the smallest possible steps.

#### Scene 1:

Torino, early evening

I am talking about rock samples again. No one interrupts me. Someone laughs; someone pours more wine. I feel understood in a strange and comforting way.

#### Scene 4:

Via WhatsApp, 2:17 AM Colombian time "Cuenta bien."

I start from the beginning. They listen. They always do.

Laughter breaks the tension. I breathe.

#### Scene 7:

My desk

A printed draft lies under a cat. Another is threatened by a dog's tail.

I accept that this is, in fact, the ideal peer review.

#### Scene 9:

His living room

Two laptops open, two people tired, one game paused for the third time.

"Hai mangiato?"

I say "no."

He hands me chocolate.

The scene resets.

#### Scene 12:

The bed

"Work from here, at least stay close."

I type. He falls asleep.

The night feels less cold.

#### **Scene 15:**

A call to Colombia

A voice says "te extraño, pero estoy orgullosa." I swallow the nostalgia, grateful for a love that survives oceans.

#### **Scene 18:**

The lab

A rock sample refuses to saturate. I consider screaming.

I don't.

Hours later it finally absorbs water, as if teaching me something about life.

#### Scene 22:

A quiet moment

I realize how many hands held me through

Friends, family, fur, warmth, patience, cariño, Italian rhythms.

I don't say it out loud, but I feel it fully.

## **Abstract**

The saturation of a rock directly affects the reliability of petrophysical measurements, since small variations in fluid distribution influence the rock-fluid interaction properties, namely effective permeability and capillary pressure.

This thesis compares three procedures for saturating sandstone core plugs: a vacuum–pressure sequence performed with a Vinci saturator, a controlled-rate injection using a permeameter for low-permeability rocks, and a continuous vacuum method implemented in a custom-made chamber. All techniques were applied to the same plugs having low, intermediate and high permeability, respectively, and water uptake was quantified gravimetrically, with pressure and flow data from the injection method used only to verify stable hydraulic conditions. The vacuum–pressure sequence proved to be the most effective way for reaching high and stable saturation levels, while the controlled-rate injection produced slightly lower values. The continuous vacuum method progressed more slowly and reached intermediate saturations, reflecting its reliance on capillary-driven imbibition under low pressure.

# Contents

Acknowledgments	1
Abstract	3
Contents	4
Tables	7
Figures	8
1. Introduction	10
1.1 Background and motivation	10
1.2 Problem statement	10
1.3 Research objectives and scope	11
1.4 Methodological approach and structure of the thesis	11
2. Theoretical Framework	13
2.1 Petrophysical fundamentals	13
2.1.1 Porosity and permeability	13
2.1.2 Capillary pressure and wettability	16
2.1.3 Interfacial tension and contact angle	18
$2.1.4~{\it Pc-kr-Sw}$ relationships and hysteresis	18
2.2 Physics of saturation in porous media	19
2.2.1 Imbibition and drainage mechanisms	19
2.2.2 Capillary equilibrium and displacement efficiency	20
2.2.3 Factors affecting fluid distribution.	20
2.3 Saturation methods	21
2.3.1 Vacuum saturation	21
2.3.2 Pressure and displacement-based saturation	22
2.3.3 Centrifugation method	23
2.3.4 Controlled-rate injection and low-permeability protocols	23
2.3.5 Practical considerations and limitations	24
2.4 Comparison and reproducibility of laboratory methods	24
2.4.1 Accuracy and repeatability metrics	24
2.4.2 Experimental uncertainty	25
2.4.3 Effect of rock heterogeneity	25
2.5 Applications for underground fluid storage	26
$2.5.1~\mathrm{CO_2}$ geological storage	26
2.5.2 H <sub>2</sub> storage in porous media	27

$2.5.3~\text{CH}_4$ and other gas storage applications	27
2.5.4 Implications for caprock integrity and reservoir characterization	27
3. Experimental Methodology	29
3.1 Materials and equipment	29
3.1.1 Sandstone core samples	29
3.1.2 Porosity and permeability characterization (Vinci PoroPerm system)	30
3.1.3 Vinci saturator setup	31
3.1.4 Controlled-rate injection saturator	32
3.1.5 Custom-made vacuum box	33
3.2 Experimental design	34
3.2.1 Rationale for selecting permeability ranges	34
3.2.2 Experimental workflow	35
3.3 Saturation protocols	36
3.3.1 Vinci saturation system / Vacuum-pressure method	36
3.3.2 Controlled rate injection method (modified CPT-350)	37
3.3.3 Continuous vacuum method (artisanal chamber)	37
3.4 Data acquisition and processing	37
3.4.1 Mass measurements	
3.4.2 Time stepped monitoring during continuous vacuum saturation	38
3.4.3 Calculation of water saturation	38
3.4.4 Processing of pressure and flow signals	38
3.4.5 Data organization for comparison across methods	39
4. Results	40
4.1 Petrophysical characterization	40
4.1.1 Porosity	40
4.1.2 Permeability	40
4.2 Vinci saturation system (Vacuum-pressure method)	42
4.2.1 Water uptake and final mass-based saturation	42
4.2.2 Qualitative observations during the vacuum stage	42
4.2.3 Observed limitations.	43
4.3 Controlled-rate injection using the threshold-pressure apparatus	43
4.3.1 Differential pressure signals and injection curves	43
4.3.2 Estimated permeability from ΔP data	45
4.3.3 Final saturation after injection	46
4.4 Continuous vacuum method (artisanal chamber)	47

4.4.1 Time-stepped outcome variables	47
4.4.2 Saturation curves and characteristic metrics	47
4.4.3 End-point saturation and gravimetric summary	47
5. Discussion	49
5.1 Interpretation of final saturations across methods	49
5.2 Influence of permeability, pore structure, and capillary effects	52
5.3 Method-dependent effects and experimental constraints	53
5.4 Integration of saturation behavior across methods	54
5.5 Implications for laboratory saturation protocols	55
6. Conclusions	57
7. References	59

# **Tables**

Table 1. Dimensions and dry masses of the sandstone plugs used in the experimental cam	paign.
	30
Table 2. Porosity results for the three sandstone plugs	40
Table 3. Klinkenberg-corrected permeability for the three plugs	40
Table 4. Gravimetric water uptake, vacuum duration, and mass-based saturation obtained	d with
the Vinci system for plugs A-C	42
Table 5. Plug A. Flow steps, differential pressure readings, and apparent permeability	45
Table 6. Plug B. Flow steps, differential pressure readings, and apparent permeability	46
Table 7. Plug C. Flow steps and resolution-limited differential pressure	46
Table 8. Final mass, water uptake, and mass-based saturation after controlled-rate injection	n46
Table 9. Plug properties and key saturation parameters for the continuous vacuum satu	ration
method	48
Table 10. Final water saturation obtained with the three methods for plugs A, B, and C	49

# **Figures**

Figure 1. Schematic representation of pore-scale viscous (green arrows) and capillary (red
arrows) forces acting during two-phase flow in a partially saturated porous medium. The blue
area represents the wetting phase (water), beige grains the solid matrix, and black regions the
nonwetting phase (air or gas)10
Figure 2. Three-dimensional pore-network segmentation of a natural sandstone sample showing
connected (red) and isolated (yellow) pore domains. Image reproduced from [10]13
Figure 3. Typical permeability-porosity relationships for sedimentary rocks. Sandstones display
a positive correlation influenced by sorting and cementation, while carbonates and shales show
broader variability related to compaction, clay content, and organic matter. Adapted from [12]
[13]
Figure 4. Conceptual representation of meniscus curvature in pore throats of different radii during
imbibition. Smaller throats (r <sub>1</sub> ) exhibit higher capillary pressures and stronger curvature than
wider throats $(r_3)$ , illustrating the inverse relationship between pore size and Pc. The concept is
based on the Young–Laplace relation described by [18]17
Figure 5. Conceptual illustration of wettability in a rock-water-air system. The contact angle and
fluid distribution vary according to the surface affinity of the rock. Although air behaves as the
nonwetting phase, it is not referred to as an "air-wet" condition but rather as a non-water-wet
case. The concept is based on the descriptions by [16]18
Figure 6. Schematic representation of the vacuum saturation of a rock sample. Adapted from [23]
Figure 7. Schematic representation of pressure-driven water saturation through a rock plug
Figure created by the author inspired by [23].
Figure 8. Photographs of the three sandstone plugs used in this study, labeled A, B, and C. The
samples differ in color, grain texture, and surface roughness, which reflects their contrasting
permeability ranges. Photo taken by the author29
Figure 9. Vinci PoroPerm apparatus. Image reproduced from [29]30
Figure 10. Actual saturation setup used in the laboratory, including the water flask, the empty trap
and the vacuum pump forming the evacuation line31
Figure 11. Simplified diagram of the vacuum pathway and the connection from the liquid tank to
the pressure vessel for filling and pressurization32
Figure 12. Photograph of the CPT-350 setup33
Figure 13. Custom-made vacuum box34
Figure 14. Schematic overview of the experimental workflow36
Figure 15. Klinkenberg plot for Plug A showing the linear fit used to obtain the Klinkenberg
corrected permeability $k^{\infty}$ 41
Figure 16. Klinkenberg plot for Plug B showing the linear fit used to obtain the Klinkenberg
corrected permeability $k$ $\infty$ 41
Figure 17. Klinkenberg plot for Plug C showing a horizontal trend consistent with negligible gas-
slip effects42
Figure 18. Differential pressure response of Plug A during controlled rate injection. The signal
shows the sequence of imposed flow steps, the associated transients, and the stable pressure
levels reached at each stage44

displays clear transitions between flow steps and stable behavior under constant flow conditions  44
Figure 20. Differential pressure response of Plug C during controlled rate injection. The $\Delta P$ trace remains within the resolution of the sensor and shows no distinguishable change across the applied flow steps
Figure 21. Mass-based water saturation curves <i>Sw</i> (t)of plugs A, B and C during continuous vacuum exposure47
Figure 22. Final water saturation obtained with the three saturation procedures (Vinci controlled-rate injection, continuous vacuum) for plugs A, B, and C
Figure 23. Final water saturation <i>Sw</i> measured in plugs A, B, and C after applying the three saturation procedures: Vinci vacuum pressure, controlled-rate injection, and continuous vacuum The grouped bars highlight how each plug responds to different saturation procedures50

## 1. Introduction

#### 1.1 Background and motivation

Getting rock samples properly prepared before any lab work often determines how reliable the petrophysical measurements will be. The method used to bring a sample to saturation sets its initial condition and in turn nudges the values obtained for key properties such as porosity, permeability and capillary pressure. Whether the goal is reservoir characterization or underground fluid storage assessment, these parameters steer flow through the pore network and help determine how faithfully laboratory data can represent processes occurring in the subsurface [1], [2]

In the past few years, as investigations into  $\mathrm{CO}_2$  and hydrogen storage have expanded, researchers have become increasingly attentive to how rock specimens become fluid saturated. Such tests demand tight control, since even small variations in gas or water content can cause a marked shift in the measured relative permeability or capillary pressure [3]. Establishing a consistent and reproducible initial saturation reduces uncertainty and supports the transfer of core-scale measurements to reservoir-scale interpretations.

Saturating a rock sample may appear straightforward at first, yet a closer look reveals the actual complications involved. During an imbibition process, fluid movement inside the pore space is controlled by the constant battle between viscous forces and capillary forces. The result depends on many variables, such as pore geometry, surface wettability and flow rate, deciding if the wetting phase advances as a continuous front or if portions of air remain trapped during its displacement. Figure 1 illustrates this interplay at the pore scale, highlighting how these competing forces shape the final distribution of fluids. Managing such a delicate equilibrium is what makes sample preparation a technically demanding process.

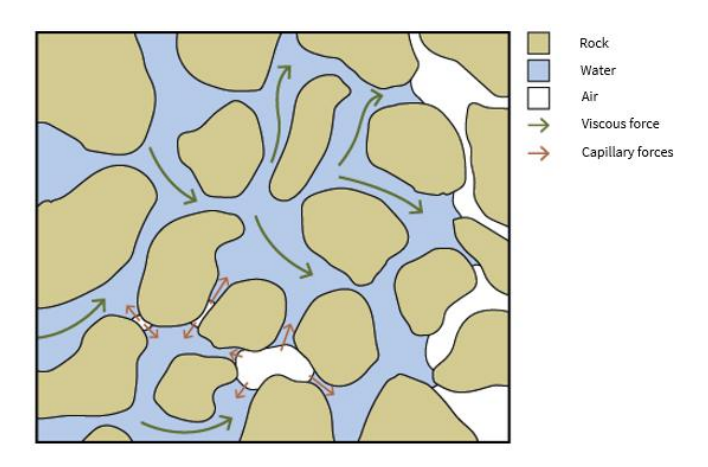


Figure 1. Schematic representation of pore-scale viscous (green arrows) and capillary (red arrows) forces acting during two-phase flow in a partially saturated porous medium. The blue area represents the wetting phase (water), beige grains the solid matrix, and black regions the nonwetting phase (air or gas).

#### 1.2 Problem statement

Several techniques have been proposed to saturate rock samples, such as vacuum impregnation, displacement under pressure, or centrifugation [4], [5]. Each method relies on a different mechanism, either through pressure gradients to force water through the pores, or centrifugal

acceleration to overcome capillary resistance, or by diffusion under vacuum conditions. However, the effectiveness of each method varies depending on the lithology, pore structure and permeability.

Low-permeability samples often present complications in reaching full saturation, due to the presence of small and poorly connected pores where residual air tends to get trapped in the form of bubbles that cannot be easily displaced. In contrast, rocks with higher permeability show fewer problems during water uptake, although they can still be sensitive to pressure fluctuations or small leaks that subtly alter the process. Because of this, results often differ considerably between laboratories even when similar methodologies are applied, especially when small procedural variations accumulate into measurable differences.

This variability represents a major constraint when comparing data or developing standardized workflows for underground fluid storage research [6], [7], [8]. As a consequence, it becomes hard to differentiate variations due to the rock properties themselves or to the way the samples were prepared. There is a need for a quantitative comparison among common laboratory saturation methods, assessing their reproducibility, limitations, and applicability to rocks with different permeability levels.

#### 1.3 Research objectives and scope

The main objective of this thesis is to compare the performance of three different laboratory techniques used for saturating three sandstone plugs before petrophysical testing. The selection of the samples reflects the permeability ranges needed for the comparison rather than any specific reservoir target. The study focuses on a commercial Vinci saturator which combines vacuum and pressure cycles, a modified CoreLab apparatus where injection rate is controlled by the user and an artisanal vacuum-water box designed to reproduce a simplified procedure.

By applying the three methods to the three samples which cover a wide range of permeability, the study aims to evaluate how each method performs across different permeability levels, allowing us to quantify the saturation reached by each method, identify the sources of uncertainty and provide practical recommendations for selecting the most appropriate method according to rock characteristics.

This analysis is limited to water saturation under laboratory conditions. Chemical reactions, multiphase flow, and long-term aging effects are not considered, yet the results can still provide useful insights for future studies on gas storage and core preparation.

Performance is evaluated through the final mass-based water saturation reached by each method, the time required to approach equilibrium, and the qualitative stability of the pressure signals during the procedure. Repeatability is assessed using the coefficient of variation of the measured saturation values and by checking whether the observed trends remain consistent across the three permeability levels.

#### 1.4 Methodological approach and structure of the thesis

The experimental work was conducted at the Environmental Park laboratories (Envipark, Turin). The study combines a theoretical review, laboratory experimentation, and a quantitative comparison of results, all structured to progressively link conceptual understanding with practical outcomes. The thesis is organized into six chapters. Chapter 2 introduces the theoretical

framework, key petrophysical principles, and the physics of saturation in porous media. Chapter 3 describes the experimental setup, materials, and procedures adopted during the laboratory activities. Chapter 4 presents the experimental results obtained from the three saturation methods, while Chapter 5 provides their comparative interpretation, discusses limitations, and identifies potential improvements. Finally, Chapter 6 summarizes the main conclusions and outlines perspectives for future research in the field.

## 2. Theoretical Framework

#### 2.1 Petrophysical fundamentals

#### 2.1.1 Porosity and permeability

Porosity and permeability are the two fundamental properties controlling how fluids move through rocks. Porosity  $(\varphi)$  represents the portion of the rock volume occupied by void spaces available for fluid storage and is expressed as a fraction of the bulk volume.

$$\varphi = \frac{V_p}{V_b}$$

where  $V_p$  is the pore volume and  $V_b$  is the bulk volume of the rock [9].

Depending on the degree of pore connectivity, porosity can be classified as absolute or effective. Absolute porosity ( $\varphi_{abs}$ ) includes all void spaces within the rock, both interconnected and isolated, while effective porosity ( $\varphi_{eff}$ ) refers only to the interconnected portion that contributes to flow.

$$\varphi_{eff} = \frac{V_{p \ interconnected}}{V_{b}}$$

From a geological point of view, porosity can result from sedimentary processes during packing and deposition, or from diagenetic processes such as dissolution and cementation, as well as from fracturing. The combination of these mechanisms determines the total storage capacity of the rock but gives no information about how easily the fluid content can move through it.

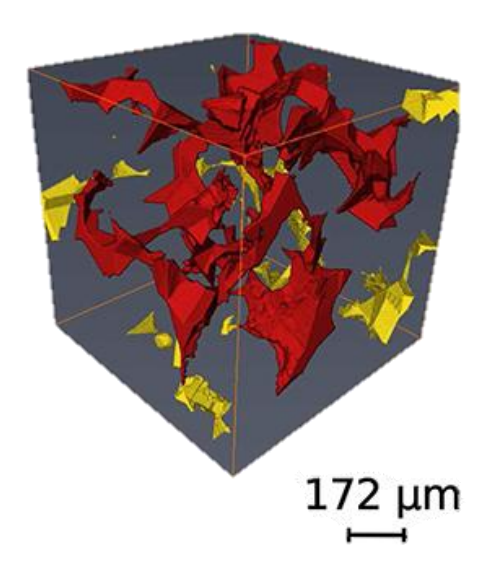


Figure 2. Three-dimensional pore-network segmentation of a natural sandstone sample showing connected (red) and isolated (yellow) pore domains. Image reproduced from [10].

A visual distinction between connected and isolated pores is shown in Figure 2 where a segmented pore network highlights how only part of the pore volume forms a continuous pathway for fluid movement.

While porosity quantifies the amount of void space in a rock, permeability relates that void space to fluid transport. According to Darcy's law, the flow rate through a porous medium is proportional to the pressure difference and inversely proportional to fluid viscosity.

$$v = -\frac{k}{\mu} \frac{dp}{dl}$$

where v is the apparent velocity,  $\mu$  is the fluid viscosity, k is the absolute permeability, and  $\frac{dp}{dl}$  is the pressure gradient [11]. Integrating Darcy's law along a sample of length L and cross-sectional area A, and using the relation v=q/A yields the standard laboratory form for volumetric flow rate q:

$$k = \frac{q\mu L}{A(P_1 - P_2)}$$

where q is the volumetric flow rate, and  $P_1$  and  $P_2$  are the inlet and outlet pressures, respectively.

Permeability mainly depends on pore distribution, tortuosity, and connectivity of the pathways. For this reason, two rocks can have the same porosity yet exhibit quite different flow responses. In addition, permeability often varies with direction, particularly in layered or fractured formations where fluids tend to follow preferential paths. These relationships are illustrated in Figure 3 which shows typical permeability–porosity trends for common sedimentary rocks.

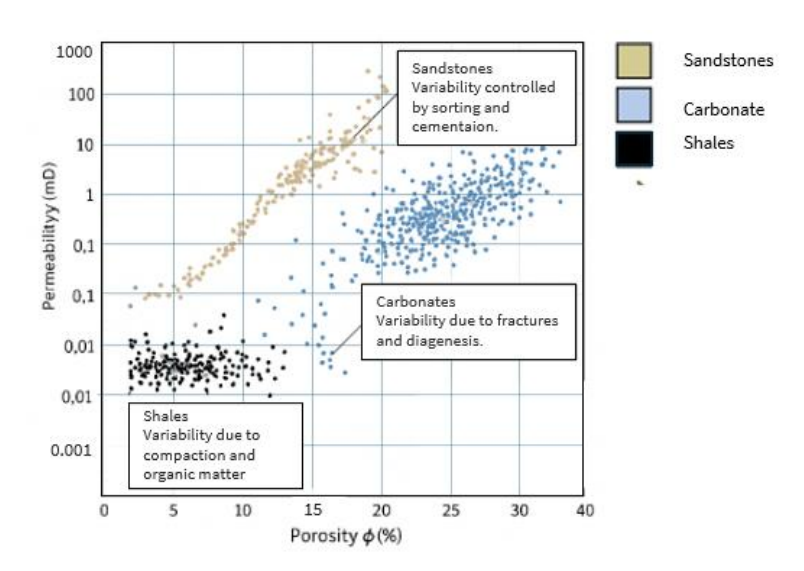


Figure 3. Typical permeability–porosity relationships for sedimentary rocks. Sandstones display a positive correlation influenced by sorting and cementation, while carbonates and shales show broader variability related to compaction, clay content, and organic matter. Adapted from [12], [13]

In petrophysical analysis, permeability is usually described in three ways. The first is absolute permeability (k) which refers to the ability of a rock to let a single fluid move through when its pores are filled. The effective permeability  $(k_{eff})$  is the one measured when more than one fluid is present, but the focus is on how easily one of them can flow while the others remain in place. Finally, relative permeability  $(k_r)$  links both concepts being the ratio between effective and absolute permeability, and it tells how much the presence of multiple fluids reduces the overall capacity for flow.

When dealing with gases, Darcy's law must be modified to account for compressibility effects, since gas density varies along with the pressure gradient. Under steady-state flow with the outlet measured at atmospheric conditions, the corrected expression for gas permeability  $(k_g)$  is given by:

$$k_g = \frac{2Q_{atm}P_{atm}\mu L}{A(P_1^2 - P_2^2)}$$

where  $Q_{atm}$  is the outlet flow rate measured at atmospheric pressure,  $P_{atm}$  is the atmospheric pressure,  $\mu$  is the gas viscosity, L is the sample length, A is the cross-sectional area, and  $P_1$  and  $P_2$  are the inlet and outlet pressures, respectively. This correction ensures that variations in gas density along the sample are correctly represented.

In rocks of low permeability, fluid motion is mostly constrained by capillary forces. Flow occurs through narrow and irregular paths, and the advance of the wetting phase is governed by slow capillary-driven imbibition rather than by viscous drag [1]. Reaching a uniform distribution of fluids can take time, often longer than predicted by basic analytical estimates.

When permeability increases, the situation changes. The internal resistance to flow gradually diminishes and viscous effects become more noticeable, although capillary forces still govern the overall displacement regime [12], [14]. Some regions still respond slowly, while others transmit fluids more easily depending on the connectivity of their pore network. In such rocks, saturation is reached faster, even when the pressure difference applied is modest, yet small heterogeneities can still delay complete equilibrium. This mixed behavior, shaped both by the pore structure and by the fluid properties, shows how strongly flow can respond to even minor shifts in pore geometry [15]

Both, porosity and permeability define the structure of the porous medium, while permeability provides the basis for understanding single-phase flow before considering the complexity of multiphase systems. Inside the pore network, fluids compete for space, and their distribution is controlled primarily by interfacial forces, even when bulk flow is present. Among these forces, capillary pressure and wettability are the most influential [2], [16]. These parameters determine which phase is forced into the smallest pores and which one occupies the broader spaces. Even minor variations can alter that equilibrium, modifying how fluids settle and how much becomes immobilized once the imposed flow stops. Although this might appear to be a strictly pore-scale effect, it ultimately controls displacement efficiency and plays a central role in the hydraulic behavior of the rock.

The following sections describe two aspects closely related to laboratory characterization: the determination of porosity by gas expansion and the correction of gas permeability for gas slippage (the Klinkenberg effect).

#### 2.1.1.1 Porosity measurement by gas expansion

Porosity in laboratory practice is often determined through gas expansion, a technique that relies on the predictable way a gas redistributes its volume when temperature is kept constant. When a known quantity of gas is allowed to expand into the evacuated pore space of a rock sample, the pressure reached at equilibrium reflects the amount of connected porosity available for flow. The procedure follows the classical Boyle–Mariotte relationship, which states that the product of pressure and volume remains constant for an ideal gas under isothermal conditions. Under

isothermal conditions, and with the sample cell initially evacuated, the gas expansion is described by the equation :

$$P_1V_1 = P_2(V_1 + V_p)$$

In practical terms, the instrument records an initial pressure in a reference cell and a final pressure once the gas has filled the accessible pores. The ratio between these two pressures, together with the known reference volume, allows the connected pore volume to be computed. Only the pores that communicate with the exterior participate in this expansion, which means that the method naturally isolates the effective porosity rather than the absolute porosity of the rock. Isolated pores remain undetected since they do not respond to the pressure pulse. Although the technique requires temperature stability and careful correction of dead volume, it provides a consistent and widely used way of quantifying the connected pore network in reservoir materials.

#### 2.1.1.2 Gas slippage and the Klinkenberg correction

When measuring permeability with gases, an additional effect comes into play. At low pressures, gas molecules do not adhere completely to the pore walls and instead slip along the surface, which increases the apparent flow rate. This phenomenon, known as gas slippage, causes permeability measured at lower mean pressures to appear higher than the intrinsic permeability of the rock. [17] showed that this effect can be corrected by expressing the apparent permeability  $k_{app}$  as a linear function of the reciprocal of the mean pressure  $P_m$ , such as:

$$k_{app} = k_{\infty} \left( 1 + \frac{b}{P_m} \right)$$

where  $k\infty$  represents the true permeability at infinite pressure and b is the slippage factor. By conducting measurements at different pressures, a linear regression of  $k_{app}$  against  $\frac{1}{P_m}$  allows  $k_\infty$  to be obtained from the intercept. This correction is particularly relevant in low-permeability rocks, where narrow pore throats magnify the influence of slip flow.

#### 2.1.2 Capillary pressure and wettability

Capillary pressure (Pc) is defined as the pressure difference at the interface between two immiscible fluids when they coexist within a porous medium. It is expressed as the pressure of the nonwetting phase minus that of the wetting phase.

$$Pc = P_{nw} - P_{w}$$

and is governed by surface tension, contact angle, and pore geometry. The classical Laplace equation [18]

$$Pc = \frac{2\gamma cos\theta}{r}$$

shows that smaller pores and higher interfacial tensions lead to higher capillary pressures. This relationship explains why saturating tight rocks is more difficult, as their small pore radii increase the resistance to fluid entry, as illustrated conceptually in Figure 4.

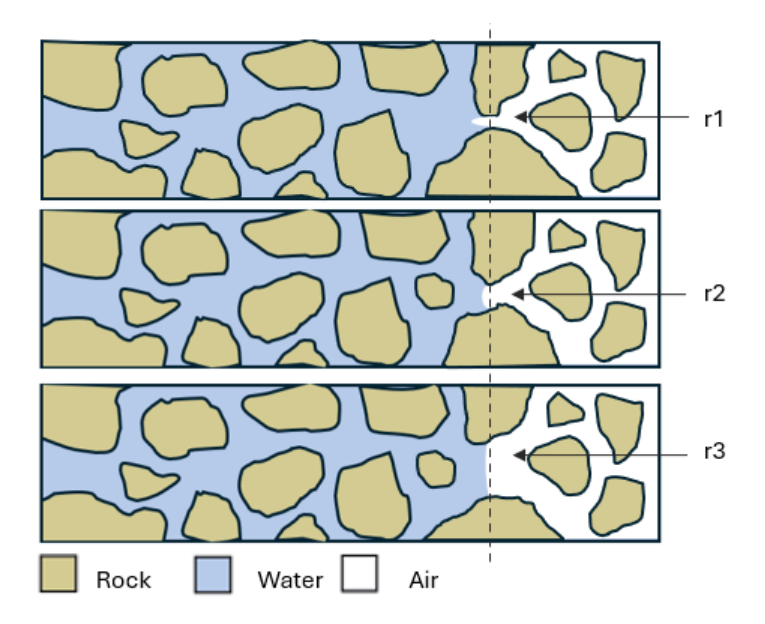


Figure 4. Conceptual representation of meniscus curvature in pore throats of different radii during imbibition. Smaller throats  $(r_1)$  exhibit higher capillary pressures and stronger curvature than wider throats  $(r_3)$ , illustrating the inverse relationship between pore size and Pc. The concept is based on the Young–Laplace relation described by [18].

Wettability is one of the main factors that determines how fluids distribute inside a rock. It describes the preference of a solid surface for one fluid over another and is usually expressed through the contact angle formed at the solid, liquid, and gas interface [16]. In water-wet systems, water tends to spread over the mineral surfaces and occupy the smallest pores. In contrast, in oil-wet or non-waterwet rocks, the nonwetting phase takes over those regions. Natural rocks rarely show a single uniform behavior. They often display mixed-wettability conditions caused by mineral heterogeneity or by previous exposure to hydrocarbons, as depicted in Figure 5 which makes the interpretation of experiments far more complex.

In laboratory conditions, both capillary pressure and wettability have a strong influence on the final saturation state. Water-wet rocks can absorb water spontaneously, even under low pressure, allowing the liquid to move easily through the pore network. Samples that are less water-wet or partially oil-wet samples tend to resist fluid entry and usually require external forces such as applied pressure or centrifugation to reach similar saturation levels. Wettability differences therefore explain why two experiments conducted under the same pressure and duration can still result in different degrees of saturation. Understanding this interfacial control is essential to evaluate the performance of vacuum and pressure-based methods and to assess the reproducibility of core preparation workflows.

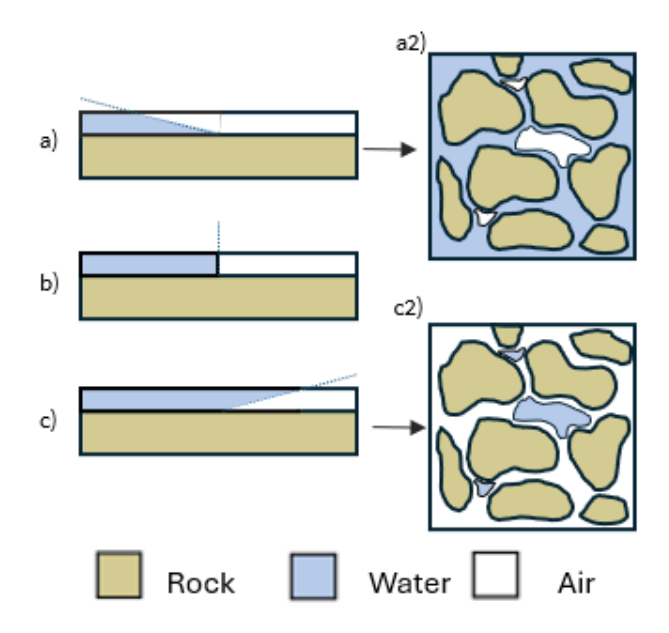


Figure 5. Conceptual illustration of wettability in a rock-water-air system. The contact angle and fluid distribution vary according to the surface affinity of the rock. Although air behaves as the nonwetting phase, it is not referred to as an "air-wet" condition but rather as a non-water-wet case. The concept is based on the descriptions by [16].

#### 2.1.3 Interfacial tension and contact angle.

Interfacial tension (IFT) is the energy required to increase the interfacial area between two fluids that do not mix. It depends on how strongly the molecules of each fluid hold together compared with how much they interact with the other phase [18]. In porous rocks, this property affects how one fluid can move or replace another. When interfacial tension is higher, capillary forces are stronger, and the movement becomes more difficult.

The contact angle  $(\theta)$  is the angle formed at the three-phase contact line where the solid surface meets the interface between two fluids. If this angle is smaller than 90 degrees, the rock is water wet. If it is larger, the surface is not wet to water. The angle can change with the minerals in the rock, with surface roughness, or because of small chemical differences between the fluids and the solid. Even small variations in interfacial tension or contact angle can significantly change capillary pressure, especially in tight or fine-grained rocks.

In the saturation stage, lower interfacial tension allows the wetting phase to advance with less resistance and reduces the stability of trapped air pockets. This reduction in IFT is usually achieved through changes in fluid chemistry, such as adding surfactants. Degassing does not reduce interfacial tension; it simply removes dissolved gases and limits bubble nucleation, which may help avoid air entrapment during saturation.

#### 2.1.4 Pc - kr - Sw relationships and hysteresis

The relationship between capillary pressure (Pc), relative permeability (kr) and saturation (S) explains how fluids interact and move within a porous medium. These three parameters are intricately linked. When saturation changes, both Pc and kr vary, defining how easily one phase can flow or replace another. Laboratory measurements of Pc - Sw and kr - Sw curves are commonly used to reproduce displacement processes and to estimate the storage and flow behavior of reservoir and storage formations [19], [20].

The reliability of Pc-Sw and kr-Sw curves depends on how the rock was saturated before testing. When the initial saturation is not properly controlled or when small air pockets remain inside the pores, the measured curves may no longer reflect the actual hydraulic behavior of the sample. This becomes more noticeable in low-permeability rocks, where even small variations in fluid distribution can lead to clear changes in pressure and flow response.

In a drainage process, the nonwetting phase progressively invades the pore system by entering the larger and better-connected pores first, displacing the wetting phase and leaving behind small pockets that it cannot fully remove. During imbibition, the wetting phase moves back into the rock and attempts to refill the porous medium, but it follows a different set of flow pathways because part of the nonwetting phase remains immobilized in narrow throats or isolated pores, and this irreversible rearrangement of the fluid configuration is what gives rise to hysteresis in the capillary–flow response of the rock. [21] described this effect through an empirical relation between the trapped nonwetting saturation and the maximum saturation reached during drainage, an approach that is still used in core analysis.

The parameters Pc, kr and Sw depend strongly on how fluids occupy the pore space at the beginning of the experiment. Having a clear and repeatable saturation step is therefore essential. The methods commonly used to reach full water saturation, such as vacuum, pressure or centrifugation, can slightly change the shape of the curves and how reproducible the results are. For this reason, the way the sample is saturated must be controlled carefully if the goal is to obtain petrophysical data that are dependable and comparable between tests or laboratories [2]. Understanding these dependencies is key for evaluating how different saturation methods influence the reproducibility of laboratory measurements, which is one of the main objectives of this study.

#### 2.2 Physics of saturation in porous media

The migration of fluids within a porous medium results from the interplay between capillary and viscous forces acting across the pore network. Saturation provides a quantitative measure of this distribution, expressing the fraction of the accessible pore volume occupied by each fluid. In water-air systems the water saturation  $S_w$  denotes the proportion of the pore space filled by the wetting phase, while the remaining volume corresponds to the nonwetting one. Although the previous section addressed the static configuration imposed by wettability and pore geometry, the dynamic evolution of saturation involves a sequence of invasion, redistribution and trapping events driven by pressure gradients and capillary forces. These mechanisms are commonly interpreted within the Pc - kr - Sw framework, which links capillary pressure, relative permeability and saturation and provides the reference basis for the description of multiphase flow in porous media [1].

#### 2.2.1 Imbibition and drainage mechanisms

Fluid movement in porous media results from the continuous interaction between capillary attraction and viscous resistance. When two immiscible fluids coexist, the wetting phase prefers the smaller pores, coating grains, and corners, while the nonwetting phase tends to occupy the larger voids. The exchange between them occurs through two main processes known as drainage and imbibition. Drainage takes place when the nonwetting phase moves forward and replaces the wetting fluid. Imbibition happens when the wetting phase enters a pore space that was previously filled with a non-wetting one.

During drainage, the advancing front does not move evenly through the pore network. It progresses only when the applied pressure becomes strong enough to overcome the entry threshold of each pore throat. As the displacement continues, small volumes of the expelled fluid remain trapped in isolated regions of the rock. Imbibition, on the other hand, depends on capillary suction. Water, which is usually the wetting phase in sedimentary rocks, can invade pores that contain gas or oil and spread along the mineral surfaces until the system reaches a new equilibrium. The efficiency of these processes depends on the geometry of the pore network, the degree of wettability, the viscosity ratio between fluids, and the local balance among gravitational, viscous, and capillary effects [22].

Drainage and imbibition rarely follow the same path twice [21]. Once a rock has been drained, reversing the pressure does not bring back the same saturation. Small amounts of the displaced fluid remain trapped in tight pores or in corners where capillary forces prevail. This path dependence explains why each sample must start from a well-defined condition before any saturation experiment. A rock that is not properly cleaned or fully dried will respond differently, since the previous fluid distribution can alter how the wetting phase moves through the pore space.

#### 2.2.2 Capillary equilibrium and displacement efficiency

Capillary equilibrium represents the condition where two immiscible fluids coexist in static equilibrium within a rock, meaning there is no net flow of either phase. It occurs when the pressure difference between the fluids equals the capillary pressure corresponding to a given saturation level. In laboratory experiments, reaching this state is essential to measure reproducible Pc - Sw and kr - Sw curves.

Reaching equilibrium is not always straightforward. In low-permeability rocks the process becomes even slower because fluids move through narrow pores where diffusion and thin films carry most of the flow. As permeability decreases, the time required for the system to stabilize increases in a very noticeable way, and this helps explain why some saturation procedures last much longer than others. Methods that keep fluids in motion, either through continuous flow or through pressure steps, tend to reduce this waiting time. Static vacuum saturation behaves differently because it depends almost entirely on slow diffusion inside the pore network, so the process advances at its own pace.

The ability of a saturation method to displace the nonwetting phase depends on how easily the wetting phase spreads inside the pore space. Factors such as connectivity, interfacial tension, viscosity, and the chosen injection rate all shape this behavior, although their combined effect becomes most visible at the pore scale. Incomplete displacement often occurs after snap-off events, when the fluid interface breaks and some portion of the nonwetting phase remains trapped in isolated pores or tight throats. Once these pockets are formed, they tend to remain in place even after long equilibration times, and they limit the saturation that the rock can realistically reach[1].

#### 2.2.3 Factors affecting fluid distribution.

Several factors influence how fluids distribute while a rock becomes saturated. The size and connectivity of the pores matter the most. When pore throats vary widely, the differences in capillary entry pressure create small zones that fill faster and others that remain dry for longer. Rocks that have a more uniform pore structure, such as well-sorted sandstones, usually take up

water more evenly than those that are poorly sorted or cemented. Wettability also shapes the pattern of fluid occupancy. In water-wet rocks, water tends to coat the grains and occupy the narrower pores, forming thin and continuous films that help the fluid climb through the network. When the rock is mixed-wet or oil-wet, those films become patchy, and air or gas can form larger, irregular clusters [12], [16].

The shape of the sample and how its pores connect can change the way fluids move. When permeability varies with direction, water does not advance in a perfectly uniform way. It tends to move along the paths that offer the least resistance and may leave some parts of the rock only partially contacted. Near the sample ends the pressure field can shift slightly, and the saturation front loses some of its uniformity. This effect is more visible in shorter plugs because the boundaries influence the flow more than one might expect. Small leaks or irregular surfaces at the fittings can also release air before the rock is fully prepared, and this modifies the saturation profile in a subtle but noticeable way. Even temperature, or the way the water has been managed can have an effect. A warmer room or poorly degassed water may alter viscosity and surface tension just enough to slow the process down or make it go too fast.

Recognizing how these factors interact is key to reproducing realistic fluid distributions during laboratory work. The physics behind saturation becomes the link between the intrinsic rock properties and the effectiveness of the methods that will be evaluated later in this study.

#### 2.3 Saturation methods

Preparing a rock sample for laboratory analysis may appear simple at first, yet bringing it to a fully saturated and stable state often proves to be one of the most demanding stages in petrophysical experimentation. The goal is to build a fluid distribution within the pore system that not only resembles natural conditions but also remains steady through repeated measurements. When this balance is achieved, parameters such as porosity, permeability, and capillary pressure can describe the hydraulic behavior of the rock with real accuracy. Over time, researchers have developed several ways to reach that condition. Some methods rely on externally applied pressure gradients, others on diffusion processes or on centrifugal acceleration. Each approach arises from a different physical principle, yet all pursue the same intention to fill the pore space as thoroughly and uniformly as possible. The selection of the method depends on the characteristics of the rock, its permeability and wettability, on the properties of the fluid employed, and on the level of experimental control that the procedure requires.

#### 2.3.1 Vacuum saturation

Vacuum saturation is the most straightforward way to bring a rock to full saturation. The principle is simple, when most of the air inside the pores is removed, the wetting fluid naturally enters once the pressure is restored. In practice, the core is placed inside a sealed chamber, and the internal pressure is gradually lowered so that air can escape from the pore space. Once the sample is covered with the wetting fluid and the system returns to atmospheric conditions, the liquid begins to move inward on its own, filling the space that was previously occupied by gas, as illustrated in Figure 6.

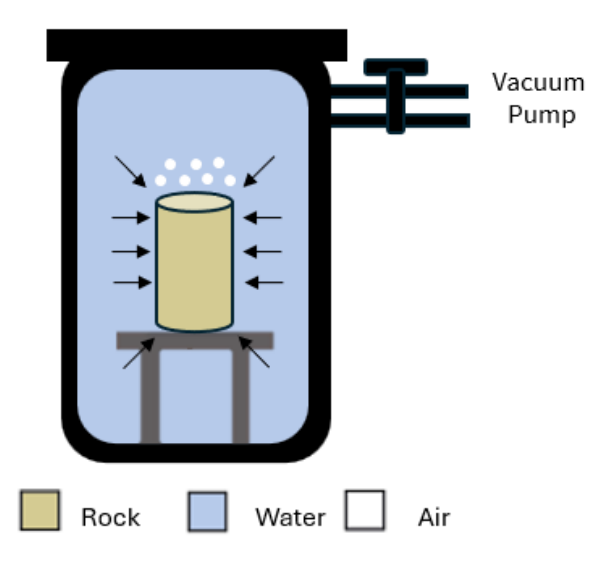


Figure 6. Schematic representation of the vacuum saturation of a rock sample. Adapted from [23].

The method performs well in rocks with moderate or high permeability where the connected pores let water move easily through the structure. In such materials, complete saturation can be reached after a few hours under vacuum. Low-permeability rocks behave differently. Even long vacuum periods leave air trapped in the smallest and most isolated pores. The result depends on details such as the vacuum strength, the duration of degassing, and how strongly the invading fluid interacts with the mineral surface [4].

Even with its limits, vacuum saturation remains a routine choice in most laboratories. It is simple to run, needs little equipment, and can be conducted with almost no supervision, which explains why it is often used during the first stages of sample preparation. Yet the outcome is never perfectly consistent. A few seconds under vacuum, a faster venting of the chamber, or a slightly different way of adding the fluid can all change how much water finally enters the pores. These variations appear small but can influence the result enough to make each test subtly unique. For that reason, vacuum saturation is usually treated as a preliminary step, a way to bring the rock close to full saturation before moving to more controlled procedures that ensure reproducible conditions.

#### 2.3.2 Pressure and displacement-based saturation

Pressure-based saturation relies on creating a controlled pressure gradient that drives the wetting fluid into the pore system of the rock. The sample is enclosed in a core holder or pressure vessel, and the fluid is injected either gradually or in steps as the pressure increases. Once the applied pressure surpasses the capillary entry threshold, the trapped air begins to give way, replaced by the advancing liquid. In most cases, this method achieves a more complete and uniform saturation than what can be attained under vacuum conditions, as illustrated in Figure 7.

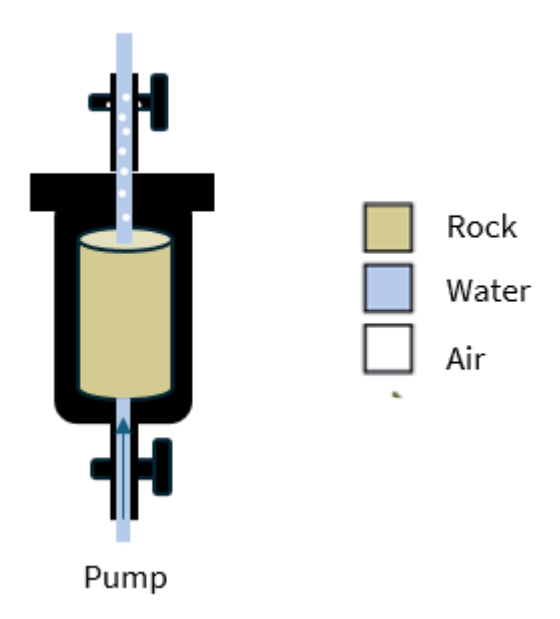


Figure 7. Schematic representation of pressure-driven water saturation through a rock plug. Figure created by the author inspired by [23].

It is particularly effective for rocks of low permeability, where diffusion alone cannot overcome capillary resistance. By carefully adjusting the injection rate and the pressure difference, the operator can steer the flow through the connected pathways and reach a steady saturation state. Depending on the purpose of the test, the process may be performed under constant pressure until equilibrium is reached, or as a continuous displacement to simulate dynamic flow.

Still, the use of pressure must be precise. If it is applied too strongly or unevenly, the internal structure of the rock may deform, and the results lose their reliability. Maintaining a balance between efficiency and preservation of the sample becomes essential. For this reason, both the injection and the confining pressures must be calibrated with care, ensuring that the system operates just above the capillary threshold without compromising the integrity of the rock [5].

#### 2.3.3 Centrifugation method

Centrifugation is another technique used to reach high saturation levels by applying centrifugal acceleration to counteract capillary resistance. During rotation, a pressure gradient develops along the core, promoting the invasion of the wetting fluid and allowing estimation of capillary pressure curves [4], [24]. The method provides fast equilibration and consistent results but requires specialized equipment and is not always effective for micro-porous materials, where extremely high rotation speeds would be necessary.

Although centrifugation offers valuable insight into fluid–rock interactions, it was not employed in this study since the focus is limited to vacuum and pressure-based saturation techniques.

#### 2.3.4 Controlled-rate injection and low-permeability protocols.

In very low-permeability samples, for instance, those around 1 mD, standard vacuum or pressure methods tend to leave small air pockets that are difficult to remove. To address this problem, studies have proposed controlled-rate injection procedures that keep a small and steady pressure difference between the inlet and the outlet, often just a few millibars. Under these gentle

conditions, the wetting fluid advances slowly through the narrowest pores and the fluid interfaces remain stable instead of collapsing or bypassing them [6], [8].

Although this study did not use these specialized systems, understanding how they work helps explain the behavior observed in the lowest-permeability plug, where capillary forces dominate and the advance of water is noticeably slower even when external pressure is applied.

#### 2.3.5 Practical considerations and limitations

Each method used to saturate rock samples works differently and performs best under certain conditions. Vacuum procedures are often chosen because they are simple and quick, especially when the goal is to prepare samples for later tests. Even in tight rocks, a fraction of the air tends to remain trapped, and it often stays there regardless of how long the test lasts. Pressure-driven methods usually remove a bit more of it, although they need a steady setup and very careful control of the injection pressure because the sample can be stressed easily if the pressure fluctuates. Centrifugation reaches equilibrium quickly and gives results that are often very consistent, but this approach depends on equipment that many laboratories simply do not have. Controlled-rate injection works at a slower pace, yet it keeps the wetting phase moving through the smallest pores in a steady way, so it becomes a good option for tight rocks even if it requires long runs and close monitoring.

No single method works equally well for all rocks. The choice depends on the type of test, the permeability range, and the level of control required by the experiment. Understanding how each technique performs and where its limitations lie provides the foundation for designing consistent laboratory workflows and for interpreting the experimental results with confidence and precision.

#### 2.4 Comparison and reproducibility of laboratory methods

Reproducibility matters because data have little value if the results cannot be compared or understood with some confidence. In saturation tests it simply refers to whether a method produces results that follow the expected physical behavior when the boundary conditions are reasonably well controlled. In principle one would check this by repeating the same test on several samples with the same properties. In practice that almost never happens. Rocks change from plug to plug, sometimes in obvious ways such as permeability, sometimes in smaller textural details that still influence the outcome.

For this reason, reproducibility is usually assessed through internal consistency. The idea is to see whether the method reacts in a steady and understandable way when it is applied to material that is broadly similar. The purpose is not to force identical saturation values but to check whether the response of the technique agrees with what is already known about the pore structure and the general behavior of the rock. A method is considered reproducible when the spread of the results can be linked to the sample or to the operating conditions rather than to changes in the procedure that were not intended. Identifying which parameters affect repeatability, and which variations simply reflect the nature of the material, helps separate the contribution of the method from variability that is inherent to the rock.

#### 2.4.1 Accuracy and repeatability metrics

The accuracy of a saturation method refers to how closely the measured saturation approaches the value that would be expected under ideal or well-defined conditions. Repeatability instead

describes how consistent the results are when the same procedure is conducted on identical or comparable samples. Together these concepts define the reliability and precision of a laboratory technique.

In core analysis repeatability is often quantified by examining the standard deviation or coefficient of variation of parameters such as porosity, permeability or saturation degree when replicate tests are available [25]. When repeated measurements are not feasible, accuracy can still be assessed indirectly through internal consistency. This may involve checking the balance between injected and retained water volumes, inspecting whether the observed trends align with expected Pc - Sw behavior or comparing the results with theoretical or previously reported values under similar conditions [2].

Methods with high repeatability tend to minimize random error and provide greater confidence in the interpretation of saturation values. Conversely large variations may indicate sensitivity to factors such as minor pressure fluctuations, incomplete degassing or nonuniform fluid entry. Recognizing these effects is essential when comparing different saturation techniques.

#### 2.4.2 Experimental uncertainty

Every saturation experiment carries a degree of uncertainty, even when the procedure appears tightly controlled. Some sources of uncertainty are systematic and come from things that are difficult to avoid, for example small calibration shifts in pressure sensors or limits in the sensitivity of the weighing system. These effects do not appear suddenly; they usually increase slowly and push the measurements in one direction over time. Other variations are random and reflect the fact that the experimental environment is never completely steady. If the injection pressure or the temperature fluctuates, even a little, or if the system needs more time to reach steady flow, the amount of water entering the sample can change. The impact is more evident in tight rocks because capillary forces take over.

Evaluating this uncertainty requires identifying which variables are most sensitive during the test and understanding how they affect the final measurements. Regular calibration of the sensors and careful determination of the sample dimensions can reduce part of the bias, although not entirely. A more persistent issue is the air or gas that becomes trapped in isolated parts of the pore network or in regions that do not fill completely. These pockets are difficult to measure directly, yet they clearly affect the apparent mass of absorbed water and, by extension, calculated properties such as porosity and effective permeability.

Since uncertainty is part of any laboratory setting, the most transparent approach is simply to report it. Indicating how stable the injection line remained, how much the balance drifted between repeated weight measurements, or how the temperature varied during the run provides context that strengthens, rather than undermines, the interpretation of the saturation results.

#### 2.4.3 Effect of rock heterogeneity

Rock heterogeneity is another factor that influences how reproducible saturation measurements can be, sometimes in ways that do not become apparent until the tests are underway. Even sandstones commonly regarded as uniform, contain subtle variations in grain size, sorting or cementation that can affect their flow behavior [4], [26]. These slight differences make it difficult to separate the response of the saturation method from the natural irregularities of the rock.

In this study the influence of heterogeneity appears in a particular form because each permeability range is represented by a single plug, and the same plug is used for all three saturation methods. Without replicating samples to average out the rock's natural variability, each plug carries its own internal texture into every measurement. As a result, the differences observed between methods must be interpreted with care. They do not necessarily reflect inconsistencies in the procedures but rather the way the plug responds according to its specific arrangement of pores and throats. Under these conditions the comparison becomes clearer when the focus is placed on the tendencies that emerge within the same plug rather than on the absolute saturation values produced by each method. This perspective provides a more grounded interpretation of the results and acknowledges that part of the variability is unavoidably tied to the character of the rock.

#### 2.5 Applications for underground fluid storage

Even when an underground storage project ultimately targets gases like  $CO_2$ ,  $H_2$ , or  $CH_4$ , the way water occupies the pore space remains a central control on how the rock later responds to gas injection. Before any nonwetting phase enters the formation, the wetting phase defines the pathways that are available, the throats that remain partially blocked, and the pockets where gas can later become immobilized. Because of this, baseline water saturation and the conditions under which a rock takes up water become essential inputs for any storage assessment. The experiments presented in this thesis do not aim to replicate reservoir multiphase flow, although they isolate the pore-scale processes that govern how water enters the pore network and how much air stays behind once the system settles.

These effects are more consequential than they may appear at first. In rocks with low or intermediate permeability even small differences in saturation efficiency modify estimates of effective porosity, usable pore volume, and the distribution of brine prior to injection. Those variations propagate into reservoir-scale predictions. Simulations require reliable saturation data to set initial fields, shape capillary pressure curves, and estimate the amount of gas that can be injected safely without forcing water into less desirable directions. For that reason a consistent laboratory workflow that compares different saturation protocols becomes a practical way to evaluate how methodological choices affect the stability and reproducibility of these parameters.

Core-scale experiments will never reproduce the full complexity of geological heterogeneity, but they capture the physics that quietly control containment at the pore level. In this sense the saturation approaches examined in this study help clarify how water uptake, trapped air, and method-specific variability translate into the parameters used to design and monitor underground fluid storage operations.

#### 2.5.1 CO₂ geological storage

When  $CO_2$  is injected into a saline reservoir the gas does not enter a clean, empty pore system. It arrives in a rock already occupied by brine, and the way this brine was arranged beforehand has a strong influence on what the gas will be able to reach. In water-wet sandstones  $CO_2$  typically finds its way into the larger pores first, while the narrow throats tend to keep small pockets of brine that refuse to drain [2]. These tiny clusters create a patchy distribution that can steer the plume in unexpected directions, slow down parts of its advance, or leave behind volumes of gas that become immobilized simply because the capillary forces are stronger than the pressure driving the injection [27]. Over long timescales these details accumulate; they end up shaping how effectively the formation stores the injected  $CO_2$ .

Laboratory saturation tests offer a way to study the physics behind these behaviors, even if the fluids used in the experiments are not  $\mathrm{CO}_2$  and brine. Watching how water enters a dry plug, how some air remains trapped after imbibition, and how sensitive this process is to permeability tells us a great deal about the capillary structure of the rock. These observations, although simple on the surface, inform the parameters that reservoir simulations depend on. Values such as water uptake, trapped air saturation, and the variability introduced by different saturation approaches help define the available pore volume, outline realistic entry pressures, and guide the shape of capillary pressure curves used in models. With these constraints in place predictions of plume movement, pressure buildup, and the strength of the caprock seal become more reliable. Without them the models drift, and uncertainty expands in ways that are difficult to correct once  $\mathrm{CO}_2$  injection is underway.

#### 2.5.2 H₂ storage in porous media

Hydrogen storage follows the general capillary logic that governs other gas-brine systems, but at the pore scale  $H_2$  behaves in ways that do not always mirror  $CO_2$ . A key difference lies in its relatively low interfacial tension with brine. That subtle shift allows hydrogen to reach pore spaces that would remain inaccessible to gases with stronger interfaces, and it makes the initial water saturation far more influential than it might seem at first glance. Small changes in how water sits within the pore structure can tilt relative permeabilities just enough to modify injectivity or the efficiency of later withdrawal, a sensitivity that has been noted in recent evaluations of cyclic storage operations [3]. For storage concepts that depend on repeated injection and production the issue becomes not only establishing an initial saturation state, but being able to recreate it with some degree of fidelity.

Laboratory saturation tests help build that understanding from the ground up. The way water enters a dry plug, the pockets of air it leaves behind, and the dependence of these patterns on permeability all reveal something about the routes hydrogen might later follow. Even though the experiments use water and air rather than hydrogen and brine, the distributions they produce still carry the imprint of the capillary structure. They hint at which pore volumes are genuinely accessible, where injectivity could weaken over time, and the conditions under which the gas might migrate in less predictable ways during cycling.

#### 2.5.3 CH<sub>4</sub> and other gas storage applications

The same ideas carry over to natural gas storage, a technology that has been used for decades but still depends on accurate knowledge of how gas and water redistribute within a reservoir. Pressure maintenance, deliverability and working gas volume all depend, in practice, on how much of the pore space is already occupied by water and on how that water redistributes when pressure conditions shift. Saturation studies at the core scale help clarify how the gas distributes between mobile and residual phases, especially in formations where heterogeneity or wettability variations can trap gas in unexpected regions [4]. These insights translate directly into estimates of how a storage site will behave after multiple injection–production cycles.

#### 2.5.4 Implications for caprock integrity and reservoir characterization

Saturation conditions influence how the rock responds in acoustic, electrical, or relative permeability tests, all of which are used to track subsurface behavior during storage operations. When the saturation state is uncertain these measurements become harder to interpret, and the uncertainty propagates into reservoir models that must predict long-term containment.

Saturation also plays a significant role in questions that go beyond storage performance, such as caprock sealing capacity and geomechanical stability. The capillary entry pressure, which defines the threshold at which a gas phase can start to invade the caprock, cannot be determined reliably unless the underlying core is prepared with care [28]. Even small amounts of trapped water or residual gas left behind during sample preparation can distort measurements such as capillary entry pressure.

For these reasons, the development of controlled and repeatable saturation procedures is not a minor methodological detail. It is part of the foundation that links laboratory observations with field-scale decisions, making it possible to trust the parameters that must be extrapolated across spatial scales. When saturation is managed with care, the transition from core-scale observation to full storage assessment becomes far more grounded and, ultimately, more trustworthy.

# 3. Experimental Methodology

The experimental work conducted in this thesis was designed to compare the performance of three laboratory saturation methods applied to sandstone core plugs spanning different permeability ranges. All procedures were performed at the Environmental Park laboratories (Envipark, Turin) under the supervision of Prof. Francesca Verga. This chapter describes the materials, equipment and workflow adopted to evaluate the efficiency, internal consistency, and practical reproducibility of the three techniques.

The workflow adopted in this study unfolded in three broad steps. Each plug was first examined to determine its basic petrophysical properties, namely porosity and permeability, so that the initial state of the material was clearly defined. The samples were then processed using the three saturation procedures, each relying on a different piece of equipment and operating sequence. Once these steps were completed, the resulting saturation levels were measured and later used as the basis for the comparative analysis. All tests took place in controlled laboratory conditions, with distilled water serving as the wetting phase; the water was degassed during the vacuum periods built into the procedures.

#### 3.1 Materials and equipment

#### 3.1.1 Sandstone core samples

The experimental work was conducted using sandstone core plugs prepared for laboratory analysis. The diameters of the samples ranged between 37.2 and 37.8 millimeters, and their lengths varied between 40.9 and 76.3 millimeters. These dimensions were compatible with the fittings and core holders available at the lab. The three plugs used in this study are shown in Figure 8 where their contrasting color, texture, and surface roughness are evident.

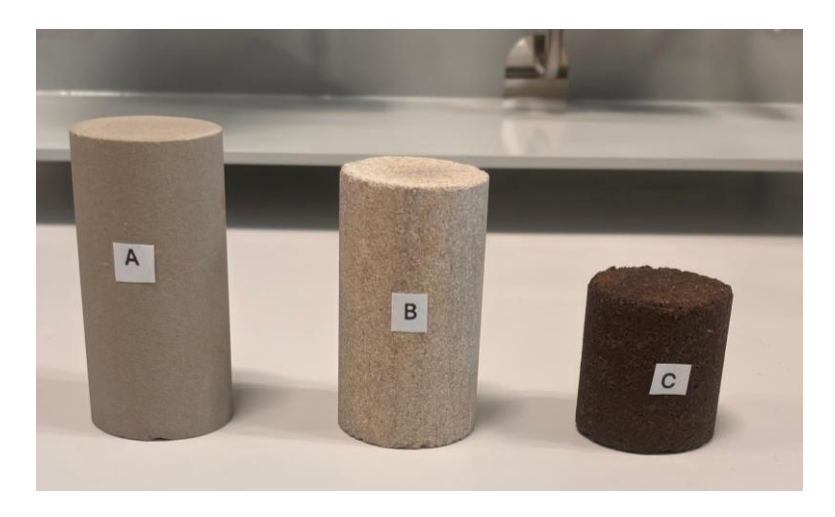


Figure 8. Photographs of the three sandstone plugs used in this study, labeled A, B, and C. The samples differ in color, grain texture, and surface roughness, which reflects their contrasting permeability ranges. Photo taken by the author.

Before use, each sample was inspected visually to confirm that the end faces were flat and free of defects. The plugs were dried in a ventilated oven at one hundred and ten degrees Celsius until their mass stabilized. After drying they were allowed to cool inside closed containers to prevent moisture uptake.

Permeability was later measured using the Vinci PoroPerm system with nitrogen gas as described in section 3.1.2. The samples were stored in sealed containers to maintain consistent initial conditions until the saturation procedures began. The dimensions and dry mass of the plugs are summarized in Table 1.

Table 1. Dimensions and			

Sample	Diameter (mm)	Length (mm)	Dry mass (g)	Notes
А	37.8	76.3	185.335	Used for low- permeability saturation tests
В	37.7	68.1	164.640	Used for medium- permeability saturation tests
С	37.2	40.9	98.487	Used for high- permeability saturation tests

#### 3.1.2 Porosity and permeability characterization (Vinci PoroPerm system)

Porosity and permeability were measured with the Vinci Technologies PoroPerm system, which integrates both measurements in a single setup and maintains consistent operating conditions across samples, as shown in Figure 9.



Figure 9. Vinci PoroPerm apparatus. Image reproduced from [29].

Porosity was obtained by allowing nitrogen to expand from a reference cell into the evacuated pore space of each plug. The instrument records the pressure variation between the cells and calculates the connected pore volume through its internal gas expansion routine. Effective porosity was computed from the ratio between this connected pore volume and the bulk volume derived from the measured dimensions.

Permeability was measured under steady nitrogen flow. The system controls the inlet pressure and records the upstream and downstream values. Apparent permeability is calculated using the

steady state form of Darcy's law, and intrinsic permeability is obtained through the Klinkenberg correction available in the PoroPerm software.

Measurements were repeated until stable readings were obtained. The system was calibrated regularly according to the Vinci operating procedure.

#### 3.1.3 Vinci saturator setup

The samples were saturated using the manual Vinci Technologies saturator, which operates through a sequence of evacuation, filling, and pressurization [30]. Each plug was placed inside a stainless-steel mesh together with metal billets that reduce the dead volume of the chamber, as shown in Figure 10.



Figure 10. Actual saturation setup used in the laboratory, including the water flask, the empty trap and the vacuum pump forming the evacuation line.

The saturation cell was connected to two containers arranged in line before the vacuum pump. The outlet of the cell was first linked to a small flask that contained a shallow layer of distilled water. This allowed visual observation of the bubbles leaving the sample during evacuation. The water flask was connected to a second empty container acting as a safety trap to prevent fluid carryover. The outlet of the trap was connected directly to the vacuum pump. as illustrated in Figure 11.

Once the cell was sealed, the vacuum pump reduced the internal pressure. Although the gauge displayed values close to minus one bar, the practical indication of complete evacuation was the absence of bubbles in the water flask. Since the distilled water used for saturation was not degassed, the disappearance of bubbles indicated that the air contained in the plug had been removed.

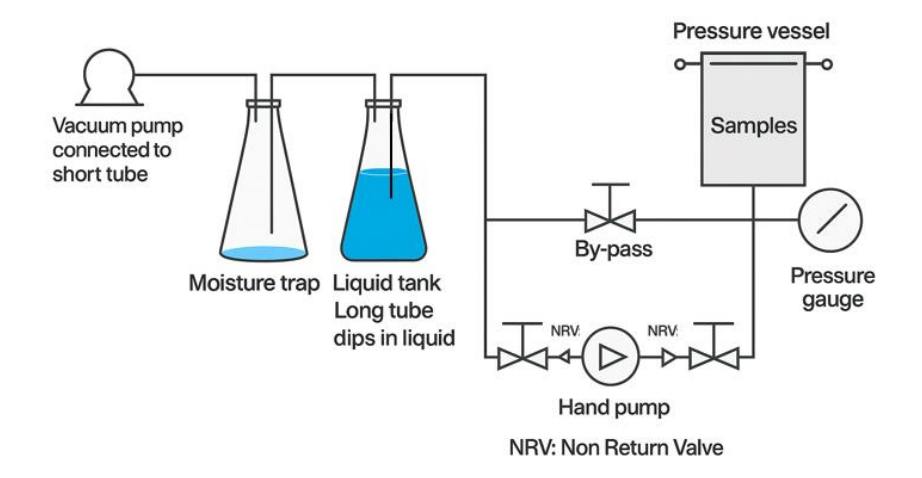


Figure 11. Simplified diagram of the vacuum pathway and the connection from the liquid tank to the pressure vessel for filling and pressurization.

After evacuation, the valve to the vacuum line was closed to isolate the system. No additional water entered the vessel at this point; the cell remained filled with the same distilled water present during evacuation. Internal pressure was then increased using the manual pump, and the analog gauge indicated values near sixteen hundred psi. At the end of the pressurization period the system was depressurized and the samples were removed and weighed.

#### 3.1.4 Controlled-rate injection saturator

A modified configuration of the Capillary Threshold Pressure Apparatus (CPT-350) was used to perform the controlled rate water injection experiments. At Envipark, the CPT-350 is normally dedicated to threshold pressure measurements, and the system integrates a metering pump and a pressure acquisition unit capable of maintaining stable flow rates, which makes the apparatus suitable for controlled injections under an adapted setup [31], as shown in Figure 12.

In this configuration the threshold pressure module of the CPT-350 was used to inject the wetting phase at a constant flow rate while the system recorded the differential pressure across the rock plug. The setup consisted of a stainless-steel hydrostatic core holder equipped with inlet and outlet pressure transducers and connected to the CPT-350 flow lines. The metering pump and the valve assembly controlled the inlet flow, and the outlet was kept at atmospheric pressure. The acquisition software of the CPT-350 recorded the instantaneous differential pressure following the routines defined for threshold pressure measurements [31].

Before each run the plug was mounted dry inside the core holder, and a confining pressure of approximately fifty bars was applied to ensure proper sleeve sealing and avoid bypass flow. The holder was then connected to the CPT-350 flow line, which had been filled with distilled water. Working with dry plugs ensured that the injection and the associated pressure response started from a fully unsaturated condition. Flow rates were set according to sample permeability, and the pressure and flow signals were acquired through the data logging system of the CPT-350 and exported for later processing.



Figure 12. Photograph of the CPT-350 setup.

#### 3.1.5 Custom-made vacuum box

A custom-made vacuum box was assembled to conduct saturation tests under continuous low pressure. The device replicates, in simplified form, the operating principle of a standard vacuum saturator, allowing the rock plugs to be exposed to a controlled vacuum and to a shallow layer of water placed at the base of the chamber.

The system consists of a transparent plastic container approximately thirty centimeters in height, closed with a removable lid fitted with a small valve connected to a vacuum pump. During operation, the chamber contains a thin layer of distilled water about three centimeters deep that acts as the wetting phase. The rock plugs are placed on a perforated support located above this water layer so that the lower surfaces remain in contact with the fluid while the upper surfaces are exposed to the low-pressure environment. An overview of the device is provided in Figure 13.

Once the chamber is sealed, the vacuum pump is switched on to reduce the internal pressure. The pressure generally stabilizes between 300 and 400 millibar. Under these conditions the air inside the pore space expands and exits as visible bubbles emerging from the surface of the plug. At the same time water is drawn gradually into the pores because of the pressure difference across the fluid interface. This produces a steady upward wetting front inside the rock as described for similar vacuum-based saturation procedures [4].

The device does not include a pressurization stage. Saturation proceeds entirely under vacuum conditions. To access the samples, the chamber can be vented to atmospheric pressure at selected intervals. Each plug may then be weighed and returned to the same position inside the box so that the procedure continues under the same operating conditions. After resealing the lid and reapplying vacuum, a short stabilization period is required for the chamber to recover the working pressure.

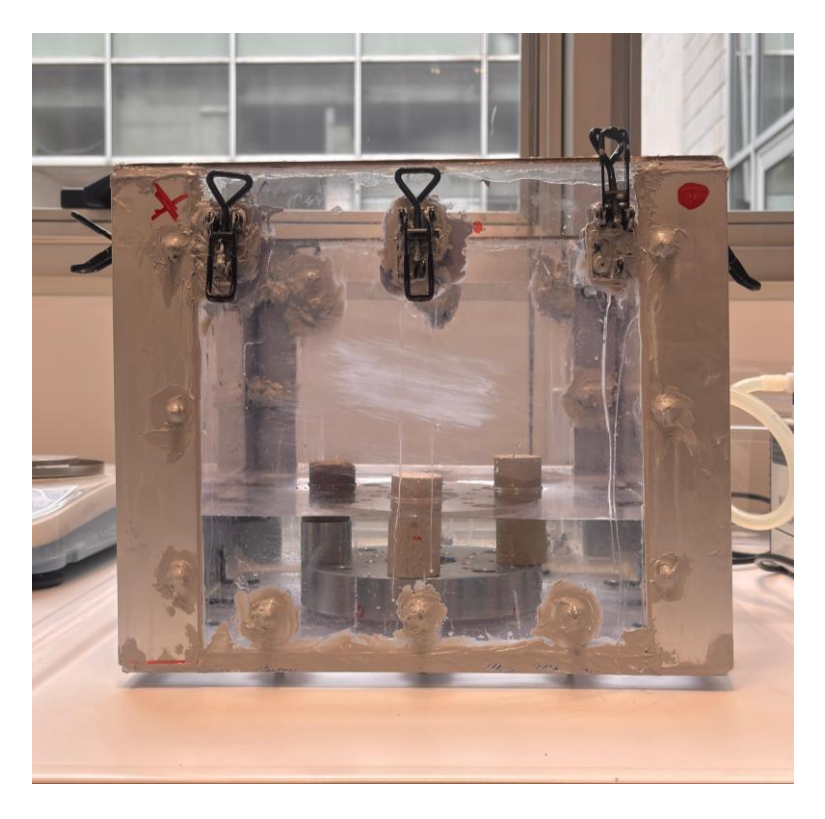


Figure 13. Custom-made vacuum box.

The vacuum box allows several plugs to be processed at the same time and provides direct visual access to bubble release and wetting front movement. The setup is suitable for stepwise saturation tests performed at constant low pressure, following approaches described in previous studies on vacuum driven saturation [6], [8]

#### 3.2 Experimental design

The experimental design of this work was developed to evaluate and compare three laboratory saturation methods applied to sandstone plugs with different permeability. The tests were planned to reproduce realistic petrophysical conditions that govern fluid displacement and to examine how permeability influences saturation behavior under distinct boundary conditions. The approach combines controlled laboratory procedures with gravimetric and hydraulic measurements to quantify water uptake and assess the stability of the resulting saturation levels.

#### 3.2.1 Rationale for selecting permeability ranges.

The three core plugs used in the study did not share the same permeability. One of them showed values near 1–2 mD, indicating that fluid movement through its pore space is strongly limited. Another plug presented permeabilities in the order of a few tens of millidarcies, which places it in a more conductive range. The remaining sample had a permeability close to 200 mD.

This permeability range was sufficient to examine how the saturation procedures behave when the rock offers different levels of resistance to flow. The three plugs therefore served as individual reference points rather than representatives of larger groups. The selected range is consistent with published values for sandstone reported in laboratory studies on saturation and drainage behavior [4], [5], [8], [32].

#### 3.2.2 Experimental workflow

The experimental campaign was arranged so that each sandstone plug was subjected to all three saturation methods, namely vacuum pressure, differential pressure injection, and continuous vacuum. Applying the full sequence to the same samples enabled direct intra sample comparison and reduced the influence of lithological variability, since each plug experienced the same set of conditions.

All experiments were conducted in a single laboratory environment under controlled temperature using the same batch of distilled water. The workflow began with sample preparation, which included drying, dimensional measurement and porosity and permeability characterization in the Vinci PoroPerm system. These measurements provided the baseline properties required to interpret the subsequent saturation stages.

After characterization, the three saturation methods were applied sequentially to each plug following the same order. The vacuum-pressure procedure was carried out first, after which the controlled-rate injection was applied using the CPT-350 system. The continuous-vacuum approach in the artisanal saturator was performed last. Keeping this order fixed prevented differences in sample history and made the results from each technique directly comparable.

After completing one method and before starting the next, the plug was brought back to the same reference condition by drying and reweighing it. This step ensured that any change in mass observed for the following procedure reflected only the saturation process under evaluation. Gravimetric measurements taken after each method provided the basis for quantifying the total water uptake of each technique. In addition to these end point measurements, the continuous vacuum stage included a dedicated time-based weighing scheme that allowed the evolution of saturation to be monitored at selected intervals. This complementary procedure made it possible to reconstruct saturation versus time curves and to identify characteristic filling times for each permeability class, adding a temporal dimension to the comparative analysis of the three methods without modifying the underlying protocols.

A schematic overview of the experimental workflow is presented in Figure 14. The diagram summarizes the sequence from initial sample characterization and through the three saturation methods applied to each plug.

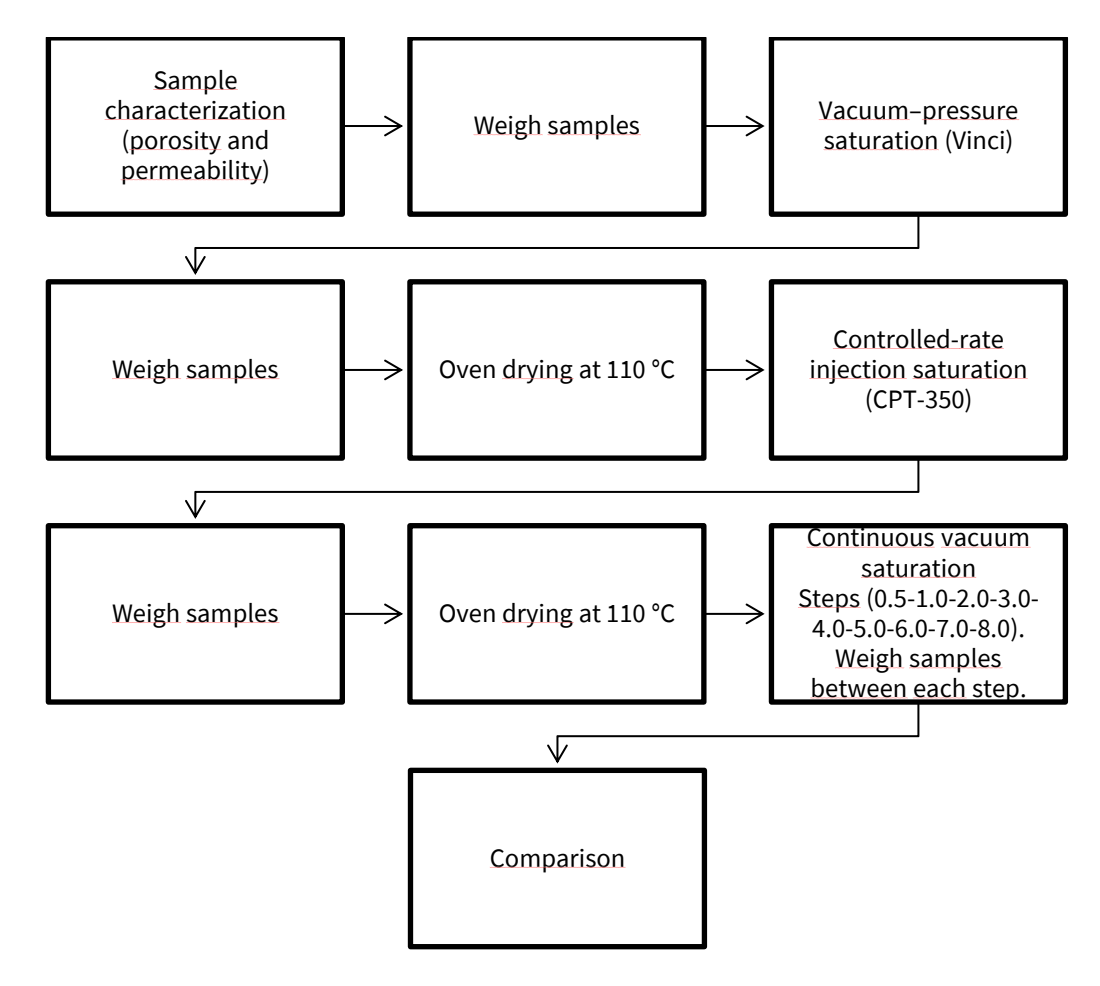


Figure 14. Schematic overview of the experimental workflow

## 3.3 Saturation protocols

## 3.3.1 Vinci saturation system / Vacuum-pressure method

Before starting the procedure, the dry plug was placed together with the billets inside the stainless-steel mesh. This assembly was then introduced into the chamber, which was filled with distilled water until fully flooded, leaving only the small voids defined by the plug and the billets.

## **Protocol**

- 1. Introduce the mesh containing the dry plug and the billets into the chamber.
- 2. Fill the chamber with distilled water until the internal volume is fully flooded, except for the small voids created by the plug and the billets.
- 3. Seal the chamber and connect it to the vacuum line.
- 4. Apply vacuum until bubble release from the plug is no longer observed in the water flask.
- 5. Maintain vacuum for an additional 30 minutes (final pressure -1 bar).
- 6. Close the vacuum valve to isolate the chamber.
- 7. Increase internal pressure manually to approximately 1600 psi.
- 8. Keep the chamber pressurized until the pressure reading becomes stable. A slight reduction in pressure typically occurs during the first minutes, after which the gauge stabilizes.
- 9. Once the pressure remains constant for 30 minutes, depressurize the chamber slowly to atmospheric conditions.
- 10. Remove the plug, allow superficial water to drain briefly, and record the saturated mass.

11. Return the plug to the oven at  $110\,^{\circ}\text{C}$  to establish dry conditions before the next saturation method.

## 3.3.2 Controlled rate injection method (modified CPT-350)

Each test began with the plug in dry condition and mounted inside the core holder under confining pressure. The aim of this method was to inject the wetting fluid at controlled flow rate while monitoring the differential pressure across the sample.

#### **Protocol**

- 1. Mount the dry plug in the core holder and apply a confining pressure of approximately 50 bar.
- 2. Fill the inlet line with distilled water and purge any residual air from the tubing.
- 3. Set the initial injection rate according to the permeability of the sample:
  - High permeability: 1–2 mL/min
  - Medium permeability: 1 mL/min
  - o Low permeability: 0.1-0.2 mL/min
- 4. Begin injection and monitor the differential pressure across the plug.
- 5. Perform short adjustments in the injection rate (within the same range) to confirm that the measured differential pressure responds consistently to the imposed flow rate and that the signal is stable.
- 6. Continue injection at the selected rate until the differential pressure becomes stable; a small initial decrease in  $\Delta P$  may occur during the first minutes.
- 7. Once  $\Delta P$  remains constant for 30 minutes, stop the injection and remove the plug.
- 8. Allow superficial water to drain briefly and record the saturated mass.
- 9. Return the plug to the oven at 110 °C to reestablish dry conditions before the next method.

## 3.3.3 Continuous vacuum method (artisanal chamber)

Each test began with the three plugs in dry condition after oven drying at  $110\,^{\circ}$ C. The plugs were placed simultaneously inside the chamber on a perforated support, with their lower surfaces in contact with a shallow layer of distilled water.

## **Protocol**

- 1. Place the three dry plugs on the perforated support inside the chamber, ensuring that the lower face of each plug is in contact with a thin water layer of approximately 3 cm.
- 2. Seal the chamber and connect it to the vacuum line.
- 3. Apply continuous vacuum until the internal pressure reaches a stable value (XX mbar).
- 4. Maintain vacuum until bubble release from all plugs becomes negligible.
- 5. Once bubbling has stopped, continue the vacuum stage for an additional 30 minutes.
- 6. Vent the chamber to atmospheric pressure, remove the three plugs sequentially, and record the mass of each sample.
- 7. Since this was the final saturation stage, no further drying was required after weighing.

# 3.4 Data acquisition and processing

The experimental campaign generated three main categories of data: gravimetric measurements, pressure and flow signals, and time resolved saturation records. All measurements were acquired under controlled laboratory conditions and processed using consistent procedures so that the three saturation methods could be compared on a common basis.

#### 3.4.1 Mass measurements

Mass determination was the primary measurement used to quantify water uptake after each saturation stage. Before the start of any method, each plug was weighed in dry condition, providing the reference mass for all subsequent calculations. After completing a saturation step, the plug was removed from the apparatus, lightly drained and weighed again using an analytical balance with a resolution of 0.001 g.

The difference between the saturated and dry masses yielded the mass of water introduced during the corresponding method. Between methods, all plugs were re dried at 110 °C until constant mass so that each procedure began from the same reproducible initial condition.

## 3.4.2 Time stepped monitoring during continuous vacuum saturation

In addition to the end point obtained after each method, the continuous vacuum setup made it possible to monitor the evolution of water uptake through time stepped measurements. At predefined intervals (for example after 1, 2, 3, 6, 8 hours), the chamber was briefly vented, and the plugs were removed one at a time, weighed and immediately returned to the vessel. Vacuum was reestablished within a few seconds, and the saturation process continued under the same conditions.

This acquisition scheme produced a sequence of mass values m(t) for each permeability class. These records allowed the construction of saturation versus time curves and provided additional information on the time required for each plug to approach its final saturation level. The procedure did not modify the underlying saturation method and was used exclusively for data collection.

## 3.4.3 Calculation of water saturation

Water saturation after each method was calculated using gravimetric formulation. The mass of water incorporated during a saturation step was determined from:

$$m_w = m_{sat} - m_{dry}$$

The corresponding water saturation was obtained as:

$$S_w = \frac{\frac{m_w}{\rho_w}}{\varphi V_b}$$

where  $\rho_w$  is the density of water at laboratory temperature,  $\varphi$  is the effective porosity measured in the Vinci PoroPerm system, and  $V_b$  is the bulk volume derived from the measured dimensions of each plug.

This approach provided a direct and consistent way to quantify and compare the degree of saturation achieved by the three methods.

# 3.4.4 Processing of pressure and flow signals

During the differential pressure method, the CPT-350 recorded the inlet and outlet pressures together with the imposed flow rate at high temporal resolution. The data were exported through the acquisition software of the CPT-350 and processed to obtain the differential pressure evolution  $\Delta P(t)$  for each plug. Since the unit integrates a metering pump and high accuracy pressure transducers, it provides the capability to control the injection rate and monitor the

corresponding hydraulic response. Although this level of control was not essential for the objectives of the present study, it offered an additional dataset that complemented the gravimetric measurements.

Under steady state conditions, apparent permeability can be estimated from the standard formulation of Darcy's law already discussed in the theoretical framework. In this work, this calculation was used only as an internal consistency check to confirm that the water injection response remained compatible with the intrinsic gas permeability obtained during initial characterization, and not as a primary objective of the experiment.

## 3.4.5 Data organization for comparison across methods

All gravimetric measurements, including both end point masses and time stepped values from the continuous vacuum stage, were compiled into a structured dataset indexed by sample identifier, permeability class, and saturation method. These gravimetric data constitute the core of the comparative analysis, since saturation was quantified directly from changes in sample mass. Pressure records obtained during the differential pressure method were stored alongside the mass measurements but were used mainly as a secondary consistency check to confirm stable flow conditions and the absence of injection anomalies. Organizing the information in this way made it possible to compare the saturation levels achieved by each method, to evaluate the time dependent filling behavior under continuous vacuum, and to ensure that all measurements remained internally coherent. This consolidated dataset forms the basis for the analysis presented in Chapter 4.

# 4. Results

# 4.1 Petrophysical characterization

### 4.1.1 Porosity

Porosity was obtained from the gas-expansion routine of the Vinci Poroperm, which provides the bulk and pore volumes of the sample before the permeability test. These quantities were taken directly from the instrument output and are reported in Table 2 together with the dry mass and nominal plug dimensions.

Plug	Diameter (mm)	Length (mm)	Dry mass (g)	Grain volume $(cm^3)$	Pore volume $(cm^3)$	Bulk volume $V_g + V_p \ (cm^3)$	Porosity (-)	Grain density $(g/cm^3)$
Α	37.6	76.3	185.335	70.330	14.280	85.624	0.169	2.635
В	37.6	68.1	164.640	61.930	13.353	76.019	0.177	2.658
С	37.2	40.9	97.819	34.710	9.743	44.453	0.219	2.837

Table 2. Porosity results for the three sandstone plugs.

Plug A and Plug B exhibit porosities near 0.17, while Plug C reaches 0.219 due to its larger pore volume relative to bulk volume. Grain densities between 2.63 and 2.84  $g/cm^3$  fall within the expected range for sandstones, confirming the internal consistency of the measurements. These values define the initial petrophysical state of the plugs and serve as the reference for the permeability and saturation analyses presented in the following sections.

For the Vinci (Section 4.2) and controlled-rate injection (Section 4.3) runs, the dry masses from Table 2 were used. Only for the continuous-vacuum run (Section 4.4) did Plug C experience a minor grain loss, for which the dry mass and volume terms were updated.

# 4.1.2 Permeability

Gas-flow permeability was measured with the Vinci Poroperm at multiple differential pressures, providing a series of apparent permeabilities  $k_{app}$  for each plug. The Klinkenberg correction yielded the liquid-equivalent permeabilities  $k_{\infty}$ , which are reported in Table 3 together with the number of points used in each fit and the corresponding coefficient of determination.

Plug	Number of points	$oldsymbol{k}_{\infty}$ (mD)	Slope (b′) (mD∙atm)	Slip factor (b) (atm)	(R <sup>2</sup> )
Α	4	1.1317	0.869	0.768	0.99
В	6	39.707	10.406	0.262	0.96
С	3	215.61	-	-	-

Table 3. Klinkenberg-corrected permeability for the three plugs.

The apparent permeabilities measured at the highest mean pressure were 1.29 mD for Plug A, 45.29 mD for Plug B and 209.39 mD for Plug C. Plug C exhibited almost no variation of  $k_{app}$  with mean pressure, indicating that gas-slip effects were negligible for this sample. Because the data

follow an essentially flat trend, a Klinkenberg regression is not physically meaningful, and no slip factor was derived. In this case, the apparent permeability measured at the highest mean pressure provides the most reliable estimate of the intrinsic permeability.

The linear regressions used to obtain the Klinkenberg-corrected permeabilities for Plugs A and B are shown in Figure 15 and Figure 16. Both datasets display a clear linear dependence of  $k_{app}$  on  $1/P_{mean}$ , which supports the reliability of the extrapolated intercepts. Figure 18 shows the data for Plug C with a horizontal trend, consistent with the negligible variation of  $k_{app}$  across the tested pressure range.

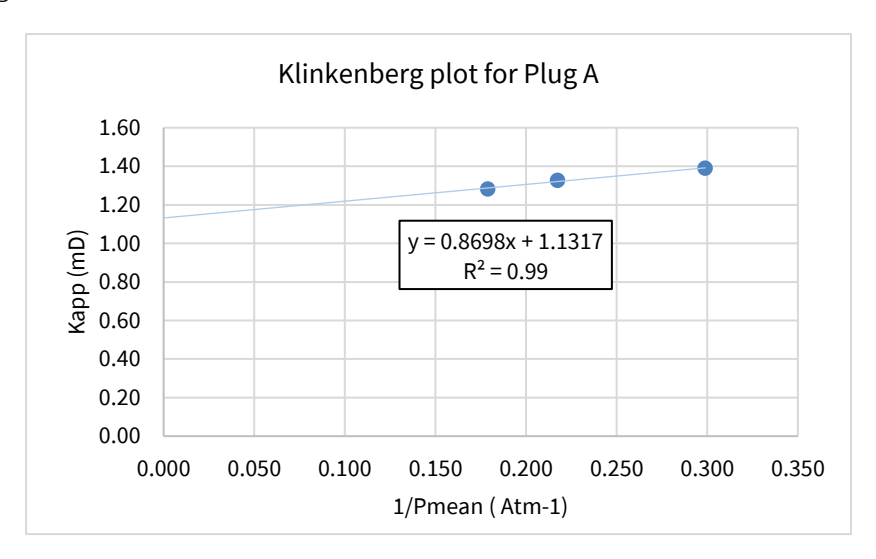


Figure 15. Klinkenberg plot for Plug A showing the linear fit used to obtain the Klinkenberg-corrected permeability  $k_{\infty}$ .

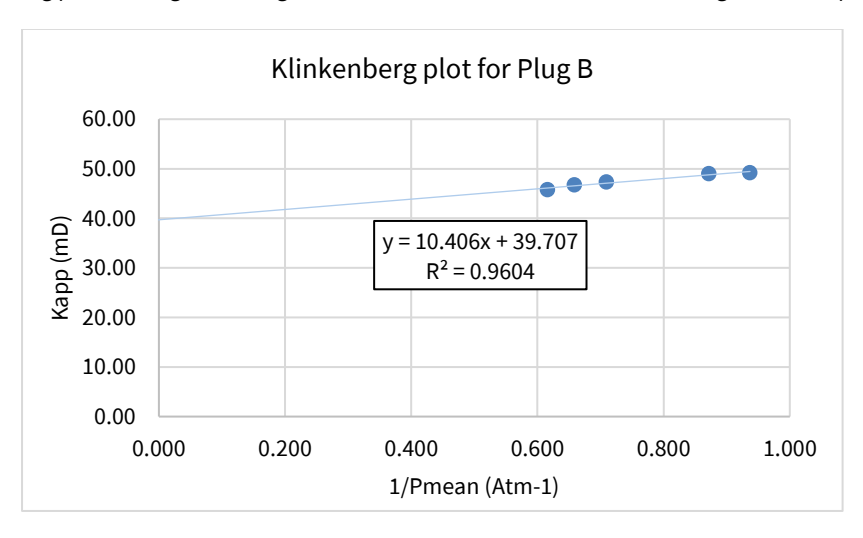


Figure 16. Klinkenberg plot for Plug B showing the linear fit used to obtain the Klinkenberg-corrected permeability  $k_{\infty}$ .

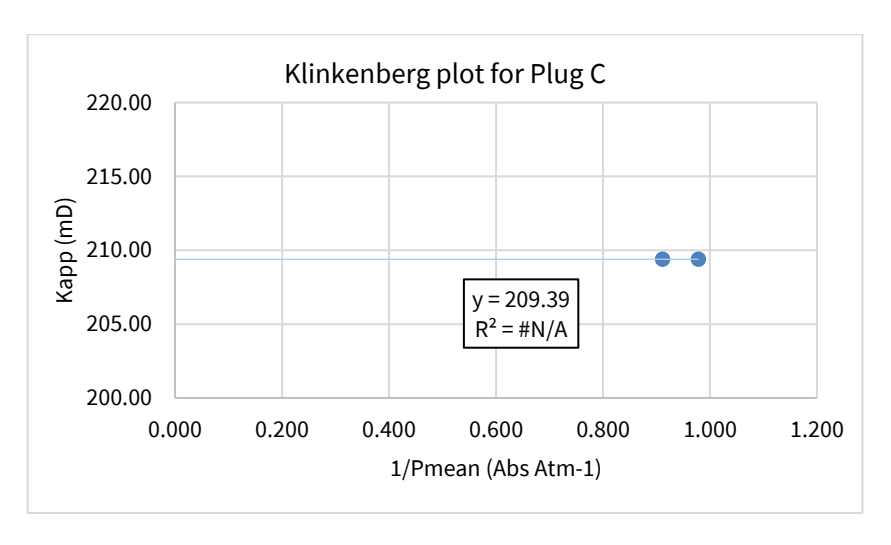


Figure 17. Klinkenberg plot for Plug C showing a horizontal trend consistent with negligible gas-slip effects.

# 4.2 Vinci saturation system (Vacuum–pressure method)

## 4.2.1 Water uptake and final mass-based saturation

The combined vacuum–pressure procedure of the Vinci system produced a clear gravimetric increase in all three plugs. Each plug gained mass relative to its dry reference state, and the corresponding water mass  $m_w$  was obtained from the difference between the final and dry masses. Mass-based water saturation  $S_w$  was obtained from the ratio of water mass to the pore volume of each plug, using the measured porosity and bulk volume. After the subsequent pressurization stage, the final gravimetric uptake showed the highest value for Plug A and the lowest for Plug C. The resulting values are reported in Table 4.

Table 4. Gravimetric water uptake, vacuum duration, and mass-based saturation obtained with the Vinci system for plugs A–C.

Plug	ф (-)	Bulk volume $V_b$ $(cm^3)$	Dry mass $m_{dry}$ (g)	Final mass $m_{sat}$ (g)	Water uptake $m_w$ (g)	Water volume $V_w \ (cm^3)$	Vacuum duration (h)	S <sub>w</sub> (-)
Α	0.179	85.624	185.335	200.460	15.125	15.171	12	0.992
В	0.185	76.019	164.640	178.611	13.971	14.013	8	0.995
С	0.219	44.453	97.819	106.526	8.707	8.733	5	0.896

All water volumes were calculated from the measured water mass using a density of 0.997 g/cm<sup>3</sup>, corresponding to the temperature at which all gravimetric measurements were performed. This value was used consistently across the three saturation procedures.

## 4.2.2 Qualitative observations during the vacuum stage

During the vacuum stage the bubbling intensity decreased progressively in all three plugs as trapped gas was displaced from the pore space. A drop in the intensity of bubbling served as a simple visual marker of how close each plug was to reaching saturation before the pressurization step. The duration of this transition differed from one sample to another. Plug A required roughly twelve hours for the release of gas to slow to isolated bubbles. Plug B displayed the same general pattern but reached that stage after about eight hours. Plug C needed approximately five hours to show a similarly stable appearance. No quantitative time series were collected during the vacuum

stage, but the progressive reduction in bubbling offered a clear visual indication of how each plug approached its pre-pressurization condition.

#### 4.2.3 Observed limitations.

The Vinci unit employs an analog pressure gauge, so pressure during the pressurization stage could only be monitored approximately and no continuous pressure record was available. The method also required removing the plug from the vessel for weighing, which introduces minor variability associated with surface drainage. In addition, the vacuum stage was tracked visually rather than through quantitative measurements, so the dataset consists of gravimetric endpoints only.

# 4.3 Controlled-rate injection using the threshold-pressure apparatus.

## 4.3.1 Differential pressure signals and injection curves

For Plug A, the differential-pressure record showed several distinct  $\Delta P$  levels that reflected the imposed flow settings. The highest  $\Delta P$  was observed during the initial flow stage. As the plug began to take in water,  $\Delta P$  shifted toward a lower level and remained there until the next change in flow. Two subsequent reductions in flow produced proportional decreases in  $\Delta P$ . Near the end of the test, increasing the flow rate led to a higher and stable  $\Delta P$  level. During all periods of constant flow, the signal remained steady, as illustrated in Figure 18.

Plug B showed a similar response. The differential pressure increased during the initial flow step, formed a pronounced maximum, and then declined toward a steady range. Raising the flow rate produced a rapid increase in the signal followed by a gradual approach to a new stable level. Returning the flow to the previous value caused a proportional decrease in pressure that remained stable for an extended period. A short increase in flow toward the end of the run produced a modest rise in differential pressure and another stable trend. Throughout the injection, the signal displayed clear step-to-step transitions and remained stable under constant-flow conditions, as shown in Figure 19.

The differential pressure record remained flat within the sensor resolution across the imposed flow steps. The signal hovered around 0.1 bar with no discernible step-to-step change while the flow rate was increased from 1.0 to 2.0 and then to 3.0 cm<sup>3</sup> min<sup>-1</sup>. No persistent oscillations were observed, and the trace remained stable for the duration of the run, as shown in Figure 20.

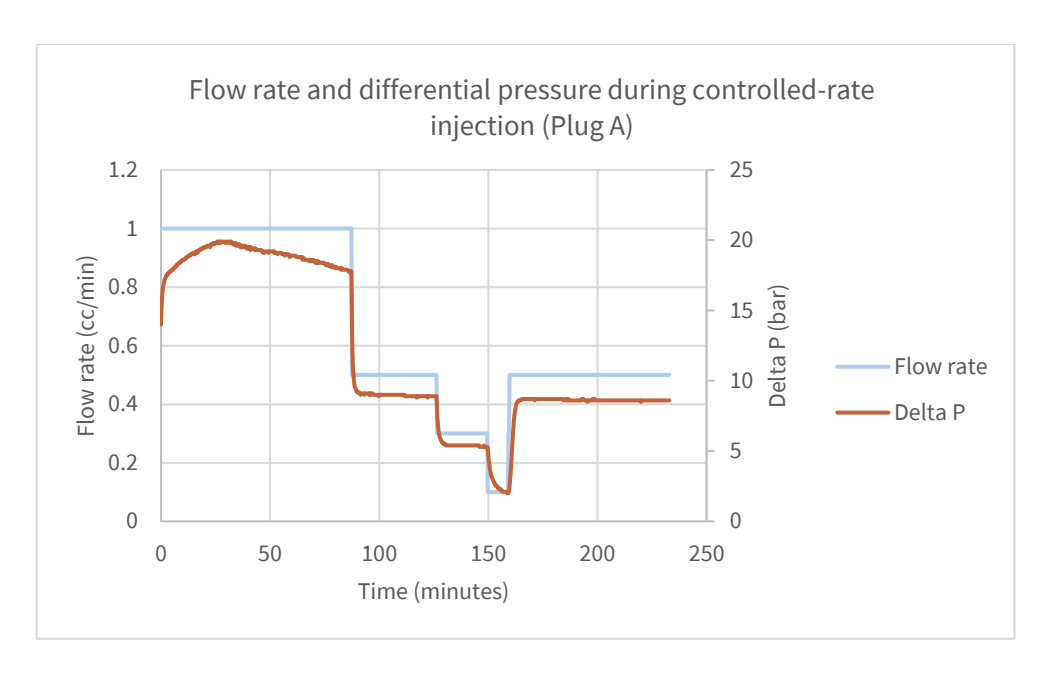


Figure 18. Differential pressure response of Plug A during controlled rate injection. The signal shows the sequence of imposed flow steps, the associated transients, and the stable pressure levels reached at each stage.

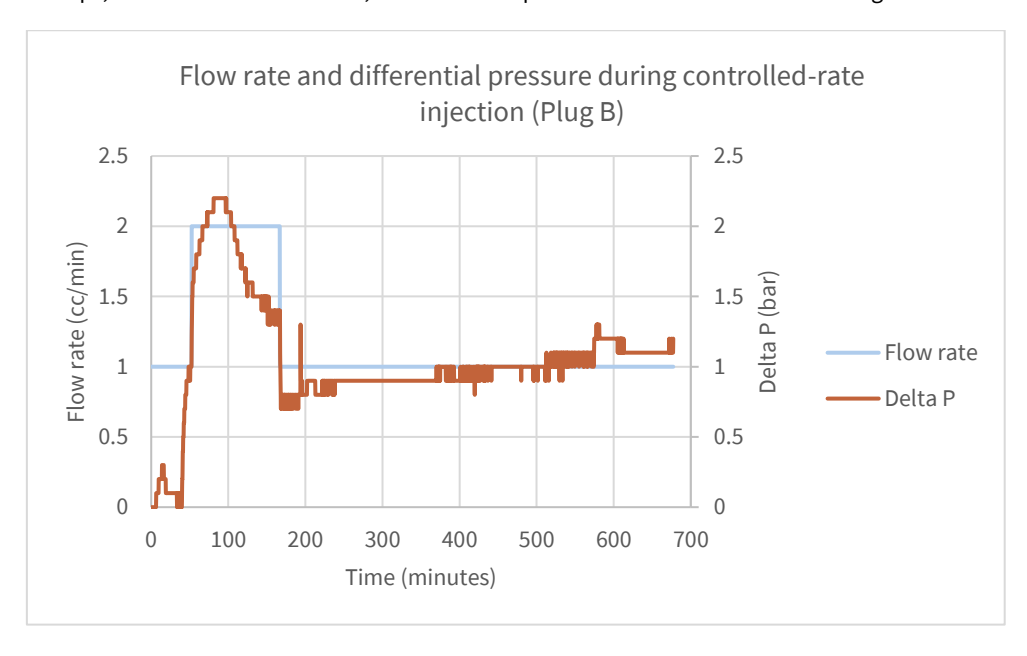


Figure 19. Differential pressure response of Plug B during controlled rate injection. The curve displays clear transitions between flow steps and stable behavior under constant flow conditions.

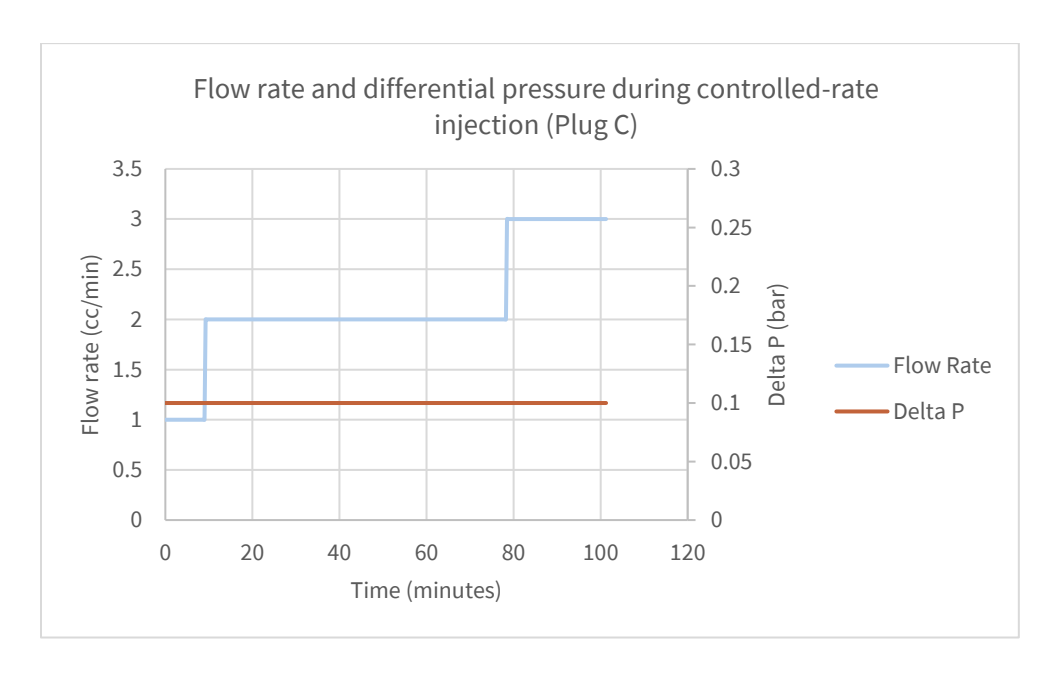


Figure 20. Differential pressure response of Plug C during controlled rate injection. The  $\Delta P$  trace remains within the resolution of the sensor and shows no distinguishable change across the applied flow steps.

## 4.3.2 Estimated permeability from ΔP data

Apparent permeability was calculated from the steady differential pressure recorded at each flow step using Darcy's equation. For consistency across all steps, the computations used the plug dimensions listed in Table 5, a water viscosity of  $9.55\times10^{-4}$  Pa s corresponding to distilled water at 22 °C, and the zero-corrected differential pressure values obtained from the injection curves. When a well-defined plateau was present, the end of that plateau was taken as the representative pressure. When the signal showed a progressive decline without a clear flat region, the final stable portion of the step was used as the representative  $\Delta P$ .

Step	Flow (q) $cm^3min^{-1}$	$\Delta P$ used (bar)	$k_{app} \ ( exttt{mD})$
1	1.00	17.8	0.676
2	0.50	8.9	0.676
3	0.30	5.3	0.682
4	0.10	2.0	0.602
5	0.50	8.6	0.700

Table 5. Plug A. Flow steps, differential pressure readings, and apparent permeability

Apparent permeability values derived from the steady differential pressure readings of Plug A show consistent results across the imposed flow steps. The estimates fall within a narrow range between 0.60 and 0.70 mD, with no irregular behavior across the different flow conditions.

For Plug B, the steady differential pressure values were obtained following the same procedure. The signal at the first flow step stabilized at about 1.00 bar once the initial rise had passed. When the flow rate was increased to  $2.00\ cm^3\ min^{-1}$ , the differential pressure reached a higher value during the transient and then declined gradually until it approached a stable reading of 1.40 bar. Returning the flow to  $1.00\ cm^3\ min^{-1}$  produced a proportional decrease in pressure, which stabilized first around 0.9 bar and then around 1.1 bar toward the end of the step. These readings were used to derive the apparent permeabilities listed in Table 6.

Table 6. Plug B. Flow steps, differential pressure readings, and apparent permeability.

Step	Flow (q) $cm^3min^{-1}$	arDelta P used (bar)	$k_{app} \ ( ext{mD})$
1	1.00	1.00	9.84
2	2.00	1.40	14.06
3	1.00	1.10	8.94

The apparent permeability values calculated for Plug B fell between 8.94 and 14.06 mD. The results remain internally consistent across the three flow steps and show no irregular behavior in the steady regions used for the calculations.

Steady differential pressure readings for Plug C were indistinguishable within the sensor resolution ( $\approx 0.1$  bar), so step-specific permeability estimates carry large relative uncertainty. The values obtained are summarized in Table 7. Values are reported as resolution-limited measurements.

Table 7. Plug C. Flow steps and resolution-limited differential pressure.

Step	Flow (q) $cm^3min^{-1}$	$\Delta P$ used (bar)	Note
1	1.00	≈ 0.1	within sensor resolution
2	2.00	≈ 0.1	within sensor resolution
3	3.00	≈ 0.1	within sensor resolution

Because  $\Delta P$  remained at the resolution floor, the calculation of  $k_{app}$  for Plug C is not reliable on a step-by-step basis. The plug is therefore excluded from the permeability comparison across flow steps, and its permeability is not reported beyond noting that  $\Delta P$  was approximately 0.1 bar under all tested flows.

### 4.3.3 Final saturation after injection

The controlled-rate injection sequence produced a measurable increase in the water content of all plugs. Plugs A and B reached high saturation levels after the injection stage, while Plug C showed a lower but still identifiable mass increase relative to its dry condition. The final masses, calculated water uptake, and mass-based saturations obtained after the injection are summarized in Table 8.

Table 8. Final mass, water uptake, and mass-based saturation after controlled-rate injection.

Plug	ф (-)	Bulk volume $V_b$ (cm $^3$ )	Dry mass $m_{dry}$ (g)	Final mass $m_{sat}$ (g)	Water uptake $m_w$ (g)	Water volume $V_w \ ({ m cm^3})$	S <sub>w</sub> (-)
Α	0.179	85.624	185.335	200.053	14.718	14.762	0.963
В	0.185	76.019	164.64	177.495	12.855	12.894	0.917
С	0.219	44.453	97.819	104.834	7.015	7.036	0.723

# 4.4 Continuous vacuum method (artisanal chamber)

## 4.4.1 Time-stepped outcome variables

The continuous vacuum method generated a time series of mass measurements for each plug, recorded at regular hourly intervals while the samples remained immersed under vacuum conditions. The variables used to track the saturation process were the instantaneous mass m(t), the incremental uptake  $\Delta m(t)$  between consecutive measurements, the cumulative water volume  $V_w(t)$  and the corresponding mass-based saturation  $S_w(t) = V_w(t)/(\phi V_b)$ . The hourly record also included a qualitative observation of the bubbling intensity, used to identify the approach to visual stability.

### 4.4.2 Saturation curves and characteristic metrics

The evolution of  $S_w(t)$  can be summarized by its overall trajectory and by simple descriptive metrics that characterize the time evolution of the process, including the initial uptake slope, the time required to reach intermediate saturation levels, and the point at which the mass increments fall within the balance resolution. These indicators allow the continuous-vacuum method to be compared with the other saturation techniques on a consistent basis, as shown in Figure 21.

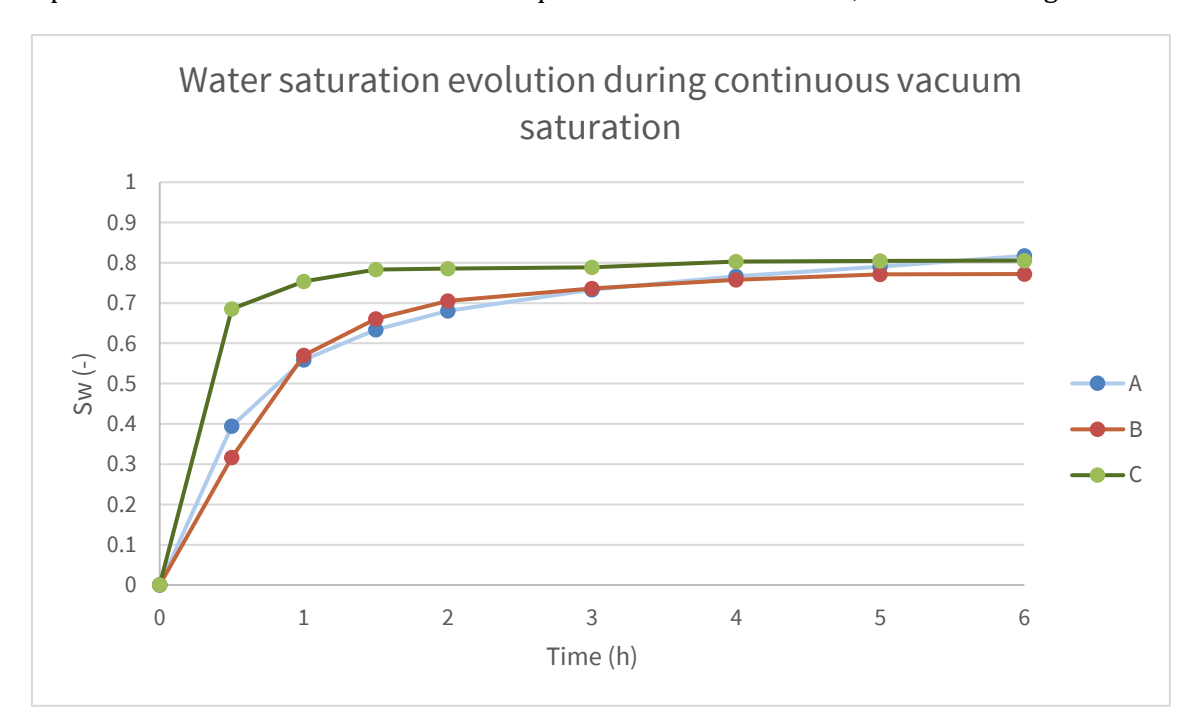


Figure 21. Mass-based water saturation curves  $S_w(t)$  of plugs A, B and C during continuous vacuum exposure.

# 4.4.3 End-point saturation and gravimetric summary

The final saturation obtained with this method is reported together with the key gravimetric quantities derived from the time series. The structure used is consistent with the reporting format adopted for the Vinci saturator and for the controlled-rate injection method. The results are summarized in Table 9.

Table 9. Plug properties and key saturation parameters for the continuous vacuum saturation method

Plug	ф (-)	Bulk volume $V_b$ (cm $^3$ )	Dry mass $m_{dry}$ (g)	<i>S<sub>w</sub></i> at time 0 (-)	$S_w$ at time 1 (-)	S <sub>w</sub> at final time (−)	Time for equilibration (h)
Α	0.179	85.624	185.335	0	0.559	0.830	7
В	0.185	76.019	164.64	0	0.570	0.772	5
С	0.219	43.864	96.524	0	0.754	0.805	4

For Plug C, a small loss of grains occurred during handling prior to the continuous-vacuum test. Accordingly, the dry-mass baseline and the bulk and pore volumes were updated for this run. The values reported in Table 9 reflect these updates.

# 5. Discussion

# 5.1 Interpretation of final saturations across methods

The three saturation procedures reached high water saturations, The three saturation procedures reached high water saturations, yet their end-point values differed across methods. Each method interacts with the pore network under a different forcing regime, which produces distinct saturation states under vacuum and pressure, gentle pressure-assisted imbibition, or purely capillary-driven invasion. Table 10 summarizes the final  $S_w$  values obtained with the three procedures and provides the reference framework for comparing their behavior.

Plug	ф (-)	/ \ \ \ \ \ \ \ \ \ \ \ \ \ \ \ \ \ \ \		Final $S_w$ Continuous vacuum
Α	0.179	0.992	0.963	0.830
В	0.185	0.995	0.917	0.772
С	0.219	0.896	0.723	0.806

Table 10. Final water saturation obtained with the three methods for plugs A, B, and C.

Notes: Final  $S_w$  values were computed using the porosity, bulk volume, and dry mass specific to each run. Only Plug C required updated dry mass and volumes for the continuous-vacuum test due to minor grain loss. Vinci and controlled-rate injection use the values in Table 2.

To help visualize the contrasts among procedures, the values in Table 10 were plotted in two complementary ways. The first representation groups the results by method and makes the separation among techniques immediately visible. The second arranges the data by plug, which clarifies how each sample responds to the three procedures. Figure 22 presents the comparison organized by method, while Figure 23 shows the same dataset grouped by plug.

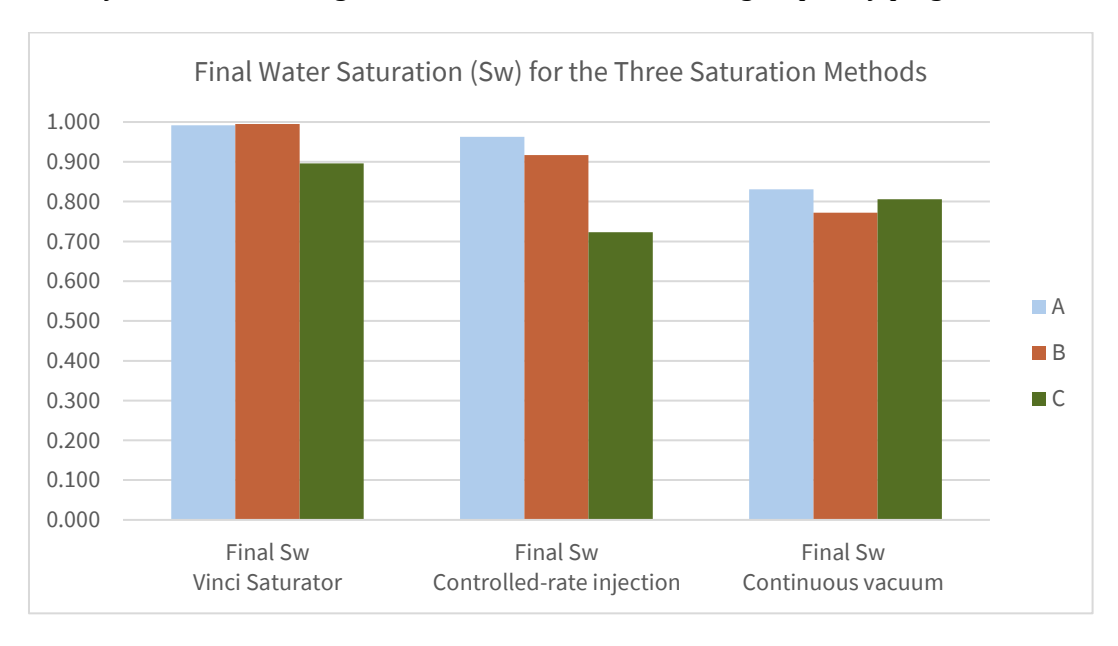


Figure 22. Final water saturation obtained with the three saturation procedures (Vinci, controlled-rate injection, continuous vacuum) for plugs A, B, and C.

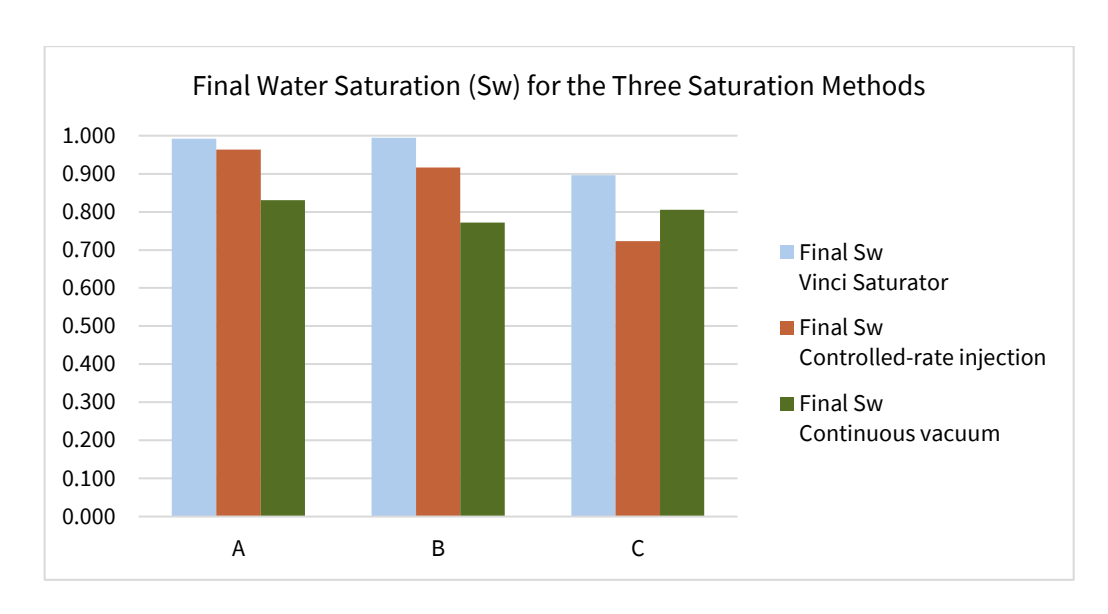


Figure 23. Final water saturation *Sw* measured in plugs A, B, and C after applying the three saturation procedures: Vinci vacuum pressure, controlled-rate injection, and continuous vacuum. The grouped bars highlight how each plug responds to different saturation procedures.

Across all samples, the vacuum pressure protocol achieved the highest water saturation. The combination of extended degassing and subsequent pressurization proved effective in displacing trapped air from both large and intermediate pore domains, consistent with the capillary entry thresholds predicted by the Laplace relation [18]. The controlled rate injection method produced similarly high saturations, though slightly lower than those obtained with vacuum pressure. This small offset suggests that forced imbibition under modest differential pressures does not fully mobilize the smallest air clusters, which aligns with classical observations on limited accessibility during gently forced imbibition [1].

The continuous vacuum procedure produced the lowest end point saturations of the three, yet its behavior fits the pore scale interpretation inferred from the other methods. Since this technique relies solely on capillarity, it tends to leave persistent gas inclusions in poorly drained pore bodies, especially in plugs where the pore network contains larger or less well-connected throats. This mechanism has been widely documented in studies of gas trapping and incomplete drainage [4]. Despite reaching lower  $S_w$  values, the continuous vacuum results are consistent and reproducible, and they reinforce rather than contradict the trends observed with the forced methods.

A first important outcome of these comparisons is that all three procedures reinforce the same dominant pore-scale controls, even though they do not produce the same ordering between plugs B and C under all forcing conditions. Forced procedures (Vinci and controlled-rate injection) follow a nearly identical trend for Plugs A and B, with the Vinci test showing Plug B reaching a slightly higher saturation than Plug A (0.995 vs 0.992), a difference within the expected measurement uncertainty. Both methods clearly separate these two plugs from Plug C, which consistently shows the lowest saturation under forced entry. This behavior confirms that pore size, rather than method-dependent effects, governs the saturation outcome across the three procedures.

Although the study does not include replicated plugs to quantify statistical dispersion, the spread among methods provides a practical measure of variability. For Plugs A and B, the difference between the vacuum pressure and controlled rate injection procedures remains below five

percentage points, showing that both techniques tend to access similar portions of the pore network. The continuous vacuum method shows a wider offset, particularly for Plug B, while Plug C exhibits the largest overall separation among techniques, with nearly eighteen percentage points between the highest and lowest values. This pattern indicates that variability arises primarily from pore throat geometry and gas retention rather than from small experimental fluctuations. This behavior also clarifies why Plug C surpasses Plug B under fully capillary driven saturation: although C ranks lower under forced procedures, its wider pore throats allow a more efficient capillary invasion than B when no viscous forcing is applied.

A closer look at plugs A, B, and C shows that their end point saturations do not scale with permeability alone. Instead, they reflect how each pore network handles capillary entry, throat connectivity, and the stability of trapped gas. Samples A and B, which have lower permeabilities but tighter and better-connected throats, continue filling even under weak forcing. Plug C, with more open throats and lower entry pressures, allows fast initial invasion but stabilizes early because larger pore bodies retain gas that cannot be mobilized by capillarity alone. This reveals that pore scale invasibility, not permeability, governs the final water uptake.

Across all samples, the vacuum pressure sequence produced the highest end-point saturations, while the continuous vacuum method consistently defined the lowest values. The controlled-rate injection results fell in between, reflecting the moderate character of its imposed pressures. These differences match the way each pore network responds to the balance between viscous and capillary forces. Plugs A and B, which contain a higher proportion of narrow and well-connected throats, continue to take in water even under weak forcing. Plug C, with larger pore bodies and lower entry pressures, fills rapidly at the beginning but stabilizes earlier because isolated gas clusters remain in poorly drained regions.

These pore-scale contrasts also explain the change in ordering between plugs B and C. Under pressure-assisted imbibition, the sequence follows A > B > C because the forced methods mobilize part of the gas held in Plug B but cannot fully drain the larger pore bodies of Plug C. Under purely capillary-driven invasion, the sequence becomes A > C > B because Plug C has wider throats that allow more efficient spontaneous entry, whereas Plug B retains gas behind constrictions that do not yield without pressure support [4], [21].

The three procedures outline a saturation envelope that reflects how each pore network responds to different forcing regimes. Continuous vacuum defines the lower limit because saturation progresses through capillary-driven invasion only, which leaves stable gas clusters in pore bodies that do not drain without pressure support. Controlled-rate injection occupies an intermediate region of the envelope, where gentle pressure-assisted imbibition mobilizes part of the trapped gas but cannot fully collapse the more stable clusters. Vacuum pressure establishes the upper bound because extended degassing and a controlled pressure gradient access pore domains that remain unreachable under weaker forcing. For these samples, the envelope follows A > B > C under forced conditions and A > C > B under purely capillary-driven invasion, a shift that reflects how throat size, pore connectivity, and gas-cluster stability govern the accessible pore volume.

Taken together, the three procedures act as complementary probes of the same pore system. Each method highlights a different portion of the accessible pore volume, but all converge toward the same pore-scale controls that determine how gas is displaced and how the wetting phase advances. This agreement indicates that the contrasts among Plugs A, B, and C originate from their

internal geometry rather than from method-dependent artifacts. The forced procedures rely on pressure-assisted imbibition, whereas the continuous vacuum test isolates capillary-driven invasion. These two displacement modes define the limits of saturation behavior and provide the foundation for the analysis that follows.

These trends define how each procedure accesses different portions of the pore space, but they do not fully explain why the plugs respond differently under similar forcing. To understand these contrasts, it is necessary to examine how permeability and pore-throat structure control the balance between viscous and capillary effects.

# 5.2 Influence of permeability, pore structure, and capillary effects

The saturation contrasts described in the previous section indicate that each procedure accesses a different fraction of the pore space, yet these method-dependent differences do not fully account for the distinct behaviors observed among plugs A, B, and C. A deeper explanation requires examining how permeability, pore throat geometry, and capillary entry conditions interact under the forcing regimes imposed by the three saturation methods. These factors control the balance between viscous and capillary effects and therefore determine how each pore network responds during water invasion.

Permeability governs how easily fluid can move through the connected pore space, but it does not control the entry conditions that determine wetting-phase invasion. These are dictated primarily by pore-throat geometry and capillary forces. The results obtained in this work indicate that the distribution and connectivity of pore throats exert a stronger influence on saturation than the absolute permeability of the samples. Rocks dominated by narrower but well-connected throats can sustain higher capillary forces and continue to draw water into the network even after the larger air volumes have been displaced, a behavior consistent with classical descriptions of spontaneous imbibition and capillary-driven invasion [1], [18]. This also affects the stability of residual gas, since throat-controlled invasion can either mobilize or retain isolated air clusters depending on their geometry, as noted in trapping studies by [21] and Pini et al. [4].

This interpretation is consistent with the hierarchy revealed by the three saturation methods. Vacuum pressure applies the strongest external forcing, controlled-rate injection imposes an intermediate level, and continuous vacuum approaches the limit of negligible viscous contribution. These differences explain why certain pore domains are accessed only under specific methods and why plugs B and C exchange their ordering when shifting from pressure-assisted imbibition to capillary-driven invasion.

The contrast among samples A, B, and C becomes clearer once permeability and saturation behavior are examined together. Plug A consistently reached the highest water saturation because, after degassing, its pore network offers little resistance to water entry. Plug B followed a similar trend, confirming that its slightly higher permeability does not hinder access to its connected pore space. Plug C behaved differently. Although it allowed rapid initial invasion, its saturation stabilized at significantly lower values, indicating that sizeable pore regions remained inaccessible or retained isolated gas clusters. This response is consistent with a pore system dominated by wider and less confining throats, where early invasion is favored but residual gas remains stable. These patterns show that the samples differ not simply in flow capacity but in how their internal geometry responds to vacuum, pressure, and gentle injection.

These differences also point to two distinct gas-trapping mechanisms. Plug C retains air because its larger pore bodies host trapped air pockets that are not displaced by capillary forces. Plug B traps air because water advances through some of its narrower throats during capillary-driven invasion, leaving air behind in regions that cannot be drained through throats with entry pressures too high for the air to pass. This distinction explains why B surpasses C under pressure-assisted conditions but falls below it when only capillary-driven invasion is active.

The behavior of the forced methods highlights complementary aspects of pore accessibility. Vacuum pressure reached the highest saturation because extended degassing removes buoyant gas clusters and the subsequent pressurization forces water into domains that remain inaccessible under weaker forcing. Controlled-rate injection applied much lower differential pressures and therefore accessed mainly the pore regions that respond to gentle viscous forcing, which explains why its final saturations, although high, remained slightly below those obtained with vacuum pressure. Continuous vacuum isolated the limits of capillary-driven invasion, and the stepwise mass measurements showed that this method consistently reached the lowest endpoint saturations of the three procedures, reflecting the persistence of trapped gas in pore domains that do not drain without external pressure gradients.

Overall, the observed saturations across samples A, B, and C show that pore-scale geometry governs the effectiveness of the saturation procedures, while the applied forcing determines how closely each method approaches the accessible pore volume. Vacuum pressure reaches the upper bound most effectively, controlled-rate injection approaches a similar state under moderate forcing, and continuous vacuum defines the lower bound set by capillary-driven invasion. The efficiency of saturation is therefore controlled by pore connectivity, small-scale capillary variations, and the stability of trapped gas rather than by permeability alone.

# 5.3 Method-dependent effects and experimental constraints

Every saturation method introduces specific measurement constraints because each technique interacts with the pore space under different forcing conditions. These constraints do not alter the intrinsic behavior of the sample s, but they influence the level of detail with which intermediate stages can be resolved and the degree of confidence that can be placed on method dependent trends. Recognizing these limitations is essential for interpreting the results consistently across procedures.

For the vacuum pressure method, the main uncertainties stem from the way pressure and saturation progress were monitored. The analog gauge provides approximate but not continuous pressure readings, and the plug must be removed from the vessel for weighing, introducing small variations associated with drainage and balance resolution. The duration of the vacuum stage was tracked visually through bubbling rather than through quantitative logging, so the approach to steady conditions can only be identified qualitatively. These limitations do not affect the gravimetric end point saturations but restrict the detail available on the intermediate evolution of the process.

For the controlled rate injection method, the dominant constraint is the limited resolution of the differential pressure sensors, which is particularly evident for Plug C. When the imposed flow rates generate  $\Delta P$  values that fall near the lower limit of the sensor, the signal cannot be separated from the background noise, which prevents extracting step-by-step permeability information. Even when  $\Delta P$  is above that limit, short transients and slow adjustments in the signal can make it

difficult to identify exactly when steady conditions are reached. For this reason, the method yields reliable final saturation values, but the pressure response during each individual step can only be interpreted in a limited way.

The continuous-vacuum procedure has a different type of constraint linked to capillary-controlled filling. Lowering the chamber pressure does not create a directed pressure gradient through the plug, so the wetting front advances without viscous forcing. The analysis therefore depends entirely on repeated mass measurements. Small changes caused by drainage, evaporation or minor balance drift can accumulate during the test and reduce the clarity of the incremental uptake. The method is well suited to capture the temporal progression of capillary-driven invasion, but its quantitative clarity depends directly on the consistency of the stepwise weighing procedure.

A further limitation of the continuous-vacuum method comes from the fact that capillary invasion only progresses if the pore network reaches the connectivity threshold required for spontaneous imbibition. In samples where some regions are poorly connected, or where throats form narrow constrictions, the wetting front may stall even though additional pore volume remains accessible under forced entry. This makes continuous-vacuum saturation particularly sensitive to subtle variations in pore connectivity, and it explains why its end-point values tend to highlight the percolation limits of each plug rather than the full pore volume that can be reached under pressure-assisted conditions.

# 5.4 Integration of saturation behavior across methods

The three saturation procedures converge toward a consistent representation of how the plugs interact with water despite their different forcing conditions. The vacuum pressure method reaches the highest end-point saturations because degassing removes the larger gas inclusions and the subsequent pressurization accesses pore regions that capillary forces alone cannot reach. The controlled-rate injection method converges toward similar values but through gentle viscous forcing, which limits the extent to which residual gas can be mobilized in larger pore bodies. The continuous-vacuum protocol complements these techniques by isolating the role of capillary forces without any directional pressure gradient, therefore revealing the fraction of the pore space that can be filled under capillarity alone. Once the data from all three methods are considered together, it becomes clear that the final saturation reflects the pore-scale geometry of the samples, while the method determines how much external energy is required to reach that state.

From an energetic standpoint, the three procedures map distinct displacement pathways. Continuous vacuum operates near the lower limit of externally supplied energy, relying almost entirely on capillary forces. Controlled-rate injection occupies an intermediate regime, where modest viscous forcing mobilizes part of the trapped gas but does not collapse the more stable clusters. Vacuum pressure establishes the upper bound, coupling degassing with a decisive pressure gradient that accesses pore domains otherwise unreachable. This energetic progression explains why the accessible pore volume increases from continuous vacuum to controlled injection and finally to vacuum pressure.

The procedures therefore differ not in the qualitative behavior of the plugs but in how closely each one approaches the intrinsic saturation potential of the rock. Sample C reaches a stable state sooner and at lower saturation under all methods, although the relative ordering between B and C depends on the forcing regime. This shift does not contradict the pore-scale interpretation;

instead, it highlights how different combinations of pore-body size, throat constriction, and gascluster stability manifest under capillary-dominated versus pressure-assisted conditions.

This integrated view shows that vacuum pressure, controlled-rate injection, and continuous vacuum probe complementary energetic windows of the same physical system: capillary-dominated invasion at the lower bound, gentle viscous forcing at an intermediate level, and forced entry establishing the upper bound of accessible saturation. Their combined behavior reinforces the interpretation that saturation efficiency is governed primarily by throat connectivity, capillarity, and gas-trapping morphology rather than by permeability alone. These convergent trends form the basis for the broader implications discussed in the following section.

# **5.5 Implications for laboratory saturation protocols**

The results indicate that vacuum pressure saturation is the most effective procedure for approaching the maximum accessible pore volume in these plugs. The combination of prolonged degassing and subsequent pressurization mobilizes gas clusters that remain stable under capillary action alone, making this method the preferred option when near complete saturation is required before permeability, or capillary pressure measurements. Vacuum saturation therefore provides the most reliable upper bound of water uptake for laboratory workflows in which the completeness of sample preparation is critical.

The controlled-rate injection method produced saturations that were marginally lower but gave a steady differential-pressure response whenever the resulting  $\Delta P$  exceeded the resolution of the sensor. This behavior shows that the method is appropriate for workflows in which saturation and permeability need to be evaluated together, provided the expected pressures can be measured accurately. The method is particularly useful when saturation needs to be coupled with stepwise permeability analysis or when monitoring the evolution of flow resistance during imbibition. Its performance also highlights the importance of matching flow-rate settings with sensor sensitivity, especially for low-permeability plugs.

The continuous-vacuum sequence isolates capillary action by removing imposed pressure gradients. It offers a controlled way to examine the portion of the pore space that fills under spontaneous imbibition. Its interpretation depends primarily on the reliability of the incremental mass measurements, but it provides valuable insight into the percolation limits of each sample and into how pore throat connectivity governs the lower bound of accessible saturation. This makes the method especially relevant for capillary-driven regimes such as primary water uptake, gas storage stability, or saturation equilibration in low permeability rocks.

Overall, the results point to a method-dependent use: vacuum-pressure saturation when the objective is to maximize water uptake, controlled-rate injection when pressure information is needed, and continuous vacuum when the interest lies in capillary-controlled filling. By combining these approaches, it becomes possible to cover the full range of saturation processes, from capillary-driven invasion to pressure assisted filling, thereby providing a more complete and physically grounded preparation strategy for petrophysical and underground storage experiments.

The main limitation of this study is the absence of replicated plugs, which prevents a quantitative assessment of variability. Future work could incorporate repeated measurements and complementary high-resolution techniques such as X-ray micro-CT or NMR to track the evolution

of gas clusters during saturation. Additional experiments under controlled boundary pressures would help refine the interpretation of the displacement pathways. Even with these limitations, the consistent behavior observed across the three methods provides a solid assessment of the tested saturation methodologies.

# 6. Conclusions

This thesis provides a rigorous experimental evaluation of three water saturation procedures applied to three dry sandstone plugs with different pore size and permeability. The saturation methods are based on distinct physical mechanisms: pressure-assisted imbibition, controlled-rate injection, and continuous vacuum saturation. The complete set of results shows that each method produces a characteristic and reproducible water saturation, confirming that the maximum saturation values depend on the adopted method and equipment. The preparation procedure determines the saturation level at which the plugs enter the subsequent laboratory tests. Since these tests assume that the samples start from a fully saturated condition, differences in the final saturation achieved by each method directly influence the reliability, comparability, and physical meaning of the measurements that follow.

The vacuum-pressure sequence was the most effective method for achieving high water saturations. Its extended degassing stage, combined with a controlled period of pressurization, reduced the amount of trapped gas and delivered consistent maximum saturation values, above 99% for the low and medium permeability plugs and above 90% for the high permeability plug. This makes it a dependable procedure for workflows that require highly saturated and uniform samples before performing subsequent petrophysical characterization.

The controlled rate injection method also produced high saturation levels, although consistently lower than those achieved with the vacuum pressure sequence. Its strength lies in the ability to acquire coherent flow and pressure data during the saturation process, allowing permeability to be estimated in the same configuration. This provides an advantage for workflows where both saturation and permeability need to be obtained without repositioning the sample, particularly when differential pressures remain within the stable resolution range of the equipment.

Continuous vacuum saturation captured the progressive filling behavior of the rock in a purely capillary-driven regime. It was useful for observing how different permeability levels correspond to variations in capillary pressure, and it helped identify differences in the relative ease of water entry across the plugs. Its main limitation was the strong dependence on equipment integrity. In this study the plastic chamber required substantial sealing where the box had been perforated for bolting, with air leakage affecting the vacuum stability and reducing reproducibility. A more robust chamber would provide a clearer view of the method's true performance.

Across all experiments the comparison reinforces a central idea. Saturation protocols shape the experimental state of the plug more than typically assumed, and their influence can overshadow intrinsic rock behavior if the method is not aligned with pore structure, rock permeability and measurement requirements. By documenting the operational domains, advantages and limitations of each procedure, this thesis provides a structured basis for designing saturation workflows that are physically grounded and experimentally consistent.

The implications extend beyond the individual configurations tested here. The results demonstrate that consistent and high-quality saturations can be obtained with different pieces of equipment when the procedure is chosen deliberately, with attention to the dominant forces acting inside the pore system. This emphasizes that saturation is not a neutral or automatic preliminary step. It is a physically governed process that needs to be designed with the same care

as the measurement itself. Connecting the practical steps performed in the laboratory with the pore scale mechanisms that control fluid entry creates more coherent datasets for applications in underground storage. The three procedures examined in this work illustrate how saturation methods can be organized and which considerations guide the selection, combination or modification of a procedure for a specific experimental objective.

#### 6.1 Recommendations

- Vacuum pressure saturation should be selected when the objective is to minimize trapped gas and to prepare samples for petrophysical measurements that require near complete and reproducible water saturations.
- Controlled rate injections are recommended for workflows in which saturation and permeability must be obtained within the same configuration, particularly for samples whose differential pressures fall within the reliable resolution range of the instrumentation.
- Continuous vacuum saturation is useful for examining capillary driven saturation paths without interference from forced flow. The method can be very useful for clayey plugs, for which the vacuum-pressure imbibition procedure is not applicable due to the very low permeability and the loss of cohesion of the material.. In this study the plastic container required extensive sealing because of bolting, which became leakage points that made the vacuum unstable. A more robust single piece chamber with sealed access ports would provide steadier operating conditions and improve reproducibility.
- For routine laboratory practice, combining vacuum exposure with a subsequent period of moderate pressurization offers an efficient and repeatable route to high quality saturations, especially in low to moderate permeability rocks.
- When comparing saturation methods across samples of different permeability, it is recommended to characterize permeability independently before selecting the saturation procedure. Aligning the saturation method with the expected capillary behavior in the rock helps reduce unwanted variability in later measurements.
- Regardless of the selected procedure, documenting the actual saturation path used and the associated pressure conditions is essential for reproducibility and for assessing whether differences in subsequent measurements arise from rock behavior or from the chosen preparation route.
- Future work should include repeated measurements on replicate plugs to isolate method-related variability from the intrinsic heterogeneity of the rock.

# 7. References

- [1] N. R. Morrow, "Physics and Thermodynamics of Capillary Action in Porous Media," *Ind Eng Chem*, vol. 62, no. 6, pp. 32–56, Jun. 1970, doi: 10.1021/ie50726a006.
- [2] S. Bachu and B. Bennion, "Effects of in-situ conditions on relative permeability characteristics of CO2-brine systems," *Environmental Geology*, vol. 54, no. 8, pp. 1707–1722, Jun. 2008, doi: 10.1007/s00254-007-0946-9.
- [3] J. Miocic, N. Heinemann, K. Edlmann, J. Scafidi, F. Molaei, and J. Alcalde, "Underground hydrogen storage: a review," *Geological Society, London, Special Publications*, vol. 528, no. 1, pp. 73–86, Aug. 2023, doi: 10.1144/SP528-2022-88.
- [4] R. Pini, S. Krevor, M. Krause, and S. Benson, "Capillary Heterogeneity in Sandstone Rocks During CO2/Water Core-flooding Experiments," *Energy Procedia*, vol. 37, pp. 5473–5479, 2013, doi: 10.1016/j.egypro.2013.06.467.
- [5] M. H. Krause and S. M. Benson, "Accurate Determination of Characteristic Relative Permeability Curves from Coreflooding Experiments with Capillary Pressure Gradients," *Adv Water Resour*, vol. 83, pp. 376–388, 2015, doi: 10.1016/j.advwatres.2015.07.009.
- [6] M. Yaralidarani and H. Shahverdi, "Co-estimation of Saturation Functions (k\_r and P\_c) from Unsteady-State Core-Flood Experiment in Tight Carbonate Rocks," *J Pet Explor Prod Technol*, vol. 8, no. 4, pp. 1559–1572, 2018, doi: 10.1007/s13202-018-0452-5.
- [7] Y. Gong, Q. Kang, R. Pawar, and H. Liu, "Two-Phase Relative Permeability of Rough-Walled Fractures," *Water Resour Res*, vol. 57, no. 12, p. e2021WR030104, 2021, doi: 10.1029/2021WR030104.
- [8] A. Mukhametdinova and others, "Characterizing Low-Permeable Shales Using Rock-Eval Pyrolysis and Nuclear Magnetic Resonance for Reconstruction of Fluid Saturation Model," *Sci Rep*, 2025, doi: 10.1038/s41598-025-15619-z.
- [9] T. H. . Ahmed, *Reservoir engineering handbook*. Gulf Professional Pub., 2010.
- [10] P.-R. Thomson, A. Aituar-Zhakupova, and S. Hier-Majumder, "Image Segmentation and Analysis of Pore Network Geometry in Two Natural Sandstones," *Front Earth Sci (Lausanne)*, vol. 6, Jun. 2018, doi: 10.3389/feart.2018.00058.
- [11] Henry Darcy, Les fontaines publiques de la ville de Dijon : exposition et application des principes à suivre et des lois à observer dans les distributions d'eau. 1856.
- [12] J. Bear, *Dynamics of Fluids in Porous Media*. New York: Elsevier, 1972.
- [13] Djebbar. Tiab and E. C. . Donaldson, *Petrophysics : theory and practice of measuring reservoir rock and fluid transport properties*. Elsevier/GPP, Gulf Professional Publishing is an imprint of Elsevier, 2016.
- [14] F. A. L. Dullien, *Porous Media: Fluid Transport and Pore Structure*, 2nd ed. Academic Press, 2012.

- [15] M. J. Blunt, Multiphase Flow in Permeable Media: A Pore-Scale Perspective. Cambridge University Press, 2017.
- [16] W. G. Anderson, "Wettability Literature Survey—Part 3: The Effects of Wettability on the Electrical Properties of Porous Media," *Journal of Petroleum Technology*, vol. 38, no. 12, pp. 1371–1378, 1986, doi: 10.2118/13934-PA.
- [17] L. J. Klinkenberg, "The permeability of porous media to liquids and gases," *Drilling and Production Practice*, no. 1945, pp. 200–213, Jan. 1941, doi: 10.5510/OGP20120200114.
- [18] A. W. . Adamson and A. P. . Gast, *Physical chemistry of surfaces*. Wiley, 1997.
- [19] A. T. Corey, "The Interrelation Between Gas and Oil Relative Permeabilities," *Producers Monthly*, vol. 19, no. 1, pp. 38–41, 1954.
- [20] N. R. Morrow, "Wettability and Its Effect on Oil Recovery," *Journal of Petroleum Technology*, vol. 42, no. 12, pp. 1476–1484, 1990, doi: 10.2118/21621-PA.
- [21] C. S. Land, "Calculation of Imbibition Relative Permeability for Two- and Three-Phase Flow From Rock Properties," *Society of Petroleum Engineers Journal*, vol. 8, no. 02, pp. 149–156, Jun. 1968, doi: 10.2118/1942-PA.
- [22] R. Lenormand, E. Touboul, and C. Zarcone, "Numerical models and experiments on immiscible displacements in porous media," *J Fluid Mech*, vol. 189, pp. 165–187, Apr. 1988, doi: 10.1017/S0022112088000953.
- [23] Nayef. Alyafei, Fundamentals of reservoir rock properties. [publisher not identified], 2018.
- [24] M. C. Leverett, "Capillary Behavior in Porous Solids," *Transactions of the AIME*, vol. 142, pp. 152–169, 1941.
- [25] "Recommended Practice for Core Analysis (API RP 40)," Washington, D.C., 1998.
- [26] Alan P. Byrnes, "Byrnes, Alan P. 'Reservoir Characteristics of Low-Permeability Sandstones in the Rocky Mountains.' The mountain Geologist 34 (1997): n. pag.," *The mountain Geologist*, 1997.
- [27] C. A. Reynolds and S. Krevor, "Characterizing Flow Behavior for Gas Injection: Relative Permeability of CO2–Brine and N2–Water in Heterogeneous Rocks," *Water Resour Res*, vol. 51, no. 12, pp. 9464–9489, 2015, doi: 10.1002/2015WR018046.
- [28] S. C. M. Krevor, R. Pini, B. Li, and S. M. Benson, "Capillary heterogeneity trapping of CO  $_2$  in a sandstone rock at reservoir conditions," *Geophys Res Lett*, vol. 38, no. 15, Aug. 2011, doi: 10.1029/2011GL048239.
- [29] ABOU MRAD Christina, "Master of Science in Petroleum and Mining Engineering BEST PRACTICES FOR PREPARATION OF SAMPLES FOR LABORATORY ANALYSIS," Torino, 2023.
- [30] VINCI Technologies, "Operating and Maintenance manual Saturator," Oct. 2013.

- [31] Vinci Technologies, "User Manual Rocks & Fluids Capillary Threshold Pressure Apparatus Operation and maintenance user manual," 2023. [Online]. Available: http://www.vincitechnologies.com
- [32] S. Bachu, "CO2 Storage in Geological Media: Role, Means, Status and Barriers to Deployment," *Prog Energy Combust Sci*, vol. 34, no. 2, pp. 254–273, 2008, doi: 10.1016/j.pecs.2007.10.001.